PERFORMANCE AND SPECIFICATION OF OPTICAL COMPONENTS WITH
MID-SPATIAL FREQUENCY SURFACE ERRORS

by

Hamidreza Aryan

A dissertation submitted to the faculty of
The University of North Carolina at Charlotte
in partial fulfillment of the requirements
for the degree of Doctor of Philosophy in
Optical Science and Engineering

Charlotte

2019

Approved by:

_____
Dr. Thomas Suleski

_____
Dr. Glenn Boreman

_____
Dr. Angela Davies Allen

_____
Dr. Christopher Evans

ABSTRACT

HAMIDREZA ARYAN. Performance and specification of optical components with mid-spatial frequency surface errors. (Under the direction of DR. THOMAS J. SULESKI)

The advent of sub-aperture computer-numerically controlled (CNC) manufacturing techniques has enabled new opportunities for high-performance optical components and systems. Freeform and other challenging designs are now possible like never before. However, such manufacturing techniques also introduce significant challenges. Mid-spatial frequency (MSF) surface errors are inherent side-effects from sub-aperture manufacturing methods that create prominent constraints on optical design, fabrication, metrology, and performance. Existing methods for specification and measurement of MSF errors in optical systems typically assume isotropic error distributions, which give misleading results for the anisotropic, structured MSF errors that are common with CNC machining.

This dissertation investigates MSF errors from three perspectives: (i) Optimization of manufacturing parameters to balance the impacts of MSF errors with manufacturing costs; (ii) Understanding effects of MSF errors on optical performance and creating analysis tools to capture these impacts; and (iii) Development of specification methods for surfaces with MSF errors. Results are addressed through three articles. The first article presents predictive models that provide a means to optimize manufacturing parameters for diamond-machined optics based on their targeted performance. The second article introduces a new, practical tool to characterize the impacts of MSF errors on performance through a novel analysis of the modulation transfer function. The third article presents a novel surface specification method for MSF errors that can be used by designers for optical tolerancing and by manufacturers for acceptance testing. The approaches introduced in the second and

the third articles provide a closed-loop for specification, testing, and tolerancing of optical surfaces with MSF errors.

DEDICATION

To my mother for her encouragement and support throughout my studies.

ACKNOWLEDGEMENTS

I would like to thank my advisor, Prof. Thomas Suleski, who guided me through this process with much support and enthusiasm. I learned a lot from our deep discussions, his great ideas and detailed problem-solving approaches, and benefited from his courses on optical design and wave optics simulation. I really enjoyed my work under his direction. I would also like to thank Prof. Glenn Boreman for his impactful contributions to this research. His profound knowledge inspired me to take the quality of this work to the next level. I also thank Prof. Angela Davis Allen for introducing me to the field of optical metrology, and helping me get started on this project and throughout my time at UNC Charlotte. I would also like to thank Prof. Chris Evans for his guidance. His vast and rigorous understanding of the subject was both helpful and motivating.

I would like to thank Alex Sohn, who gave me the opportunity at Facebook Reality Labs to dig deeper in freeform metrology, design, and fabrication. Our great discussions helped me to better understand the advances and challenges in this field and expand my skills. I would also like to thank Prof. Jannick Rolland (Univ. of Rochester) for her encouragement, Prof. Miguel Alonso and Kevin Liang (Univ. of Rochester) for collaborations, and Prof. Greg Forbes, Prof. Brigid Mullany, and Prof. Matt Davies (UNC Charlotte) for useful discussions. Last but not least, I would like to thank all my friends at UNC Charlotte who made this journey enjoyable and memorable.

TABLE OF CONTENTS

CHAPTER 1: INTRODUCTION

 1.3.1 Point Spread Function (PSF)

 1.3.2 Strehl ratio (SR)

 1.3.3 Encircled Energy

 1.3.4 Modulation Transfer Function (MTF)

 1.4.1 Power Spectral Density

 1.4.2 Bandlimited RMS

 1.4.3 Surface Slope

CHAPTER 2: PREDICTIVE MODELS FOR STREHL RATIO OF DIAMOND MACHINED OPTICS

CHAPTER 5: CONCLUSION

LIST OF TABLES

LIST OF FIGURES

LIST OF ABBREVIATIONS

BRDF   Bidirectional Reflectance Distribution Function

CNC   Computer Numerical Control

EER   Encircled Energy Radius

HSF   High Spatial Frequency

LSF   Low Spatial Frequency

MSF   Mid Spatial Frequency

MTF   Modulation Transfer Function

MMC   Minimum Modulation Curve

PSF   Point Spread Function

PSD   Power Spectral Density

PRP   Polar RMS Plot

PV   Peak to Valley

RMS   Root Mean Square

SF   Structure Function

SR   Strehl Ratio

CHAPTER 1: INTRODUCTION

1.1 Mid-Spatial Frequency surface errors

Mid-Spatial Frequency (MSF) surface errors are residual structures inherent to sub-aperture manufacturing techniques [1-7]. These errors are difficult to remove by polishing methods, and available polishing techniques can result in additional MSF errors and are not applicable to all situations. As it comes from their name, MSF errors cover the spatial frequency region between Low-Spatial Frequency (LSF) and High-Spatial Frequency (HSF) errors, as illustrated in Fig. 1-1 [8].
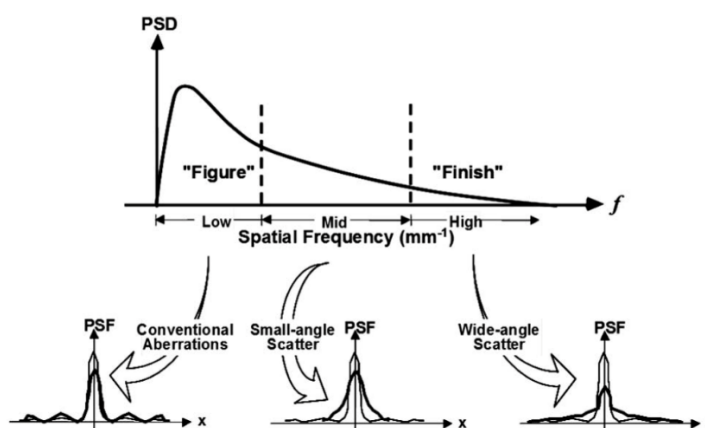
Figure 1-1: Different spatial frequency regions and their impact on the image quality [8].

The exact definition of spatial region of these errors can vary based on the application and their impact on optical performance. LSF 'figure' errors broaden the main peak of the Point Spread Function (PSF) of an optical system, and can be described for example, by the first 37 Standard Zernike polynomials [9]. HSF errors impact the performance by scattering the incident light at high angles, and traditionally have been treated by scattering theory [8].

The lower limit of HSF errors (which is the upper limit of MSF errors) has been suggested to be where the Fresnel length of the ripples is less than 1/10th of the optical path distance from a given surface to the image plane [9]. In contrast, MSF errors, which are the primary focus of this dissertation, scatter light out of the main PSF peak but at angles small enough to illuminate the focal plane [10]. Therefore, these errors lead to different image artifacts and degrade optical performance [10-13]. Also, the anisotropic structure of these errors re-shape the illumination pattern and, if large enough, could result in additional impacts on performance. Figure 1-2 shows several examples of interferometrically measured MSF errors. Notice the structured and anisotropic nature of MSF errors in these examples.
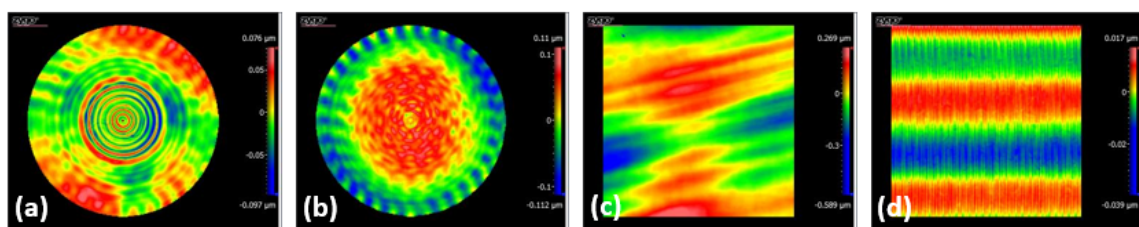
Figure 1-2: Different types of MSF errors on surfaces made through different processes; measured by (a, b) THALES. (c, d) UNC Charlotte.

The study of MSF errors can be divided into three categories. First, studies related to the impact of MSF errors on optical performance. The impact of the tool signature can be categorized into those of a random distribution and those with a structured component [13]. Assuming isotropy, Youngworth and Stone have developed simple methods that could be used for estimating the effect of MSF errors on optical performance [9, 14]. Another instance, for isotropic surfaces, is the approach through scattering theory and the BRDF of a part, which mainly aims to connect the BRDF to the Power Spectral Density (PSD) of surface errors [15-20]. Much of the theory for scattering from optical surfaces is based on

works from the early 1960's [21]. Early studies on the impact of sub-aperture fabrication tool errors date back to evaluation of surface quality of diamond turned optics by Church and Zavada in 1975 [22]. However, their statistical approach requires that perturbations are small, and errors are random with no structured spatial frequencies in the PSD [23]. Marioge and Slansky considered the impacts of structured rotationally periodic waviness on image quality in 1983 [24]. More recently, Tamkin [11-13] considered impacts of structured MSF errors on the PSF and MTF. The errors in these studies are considered to be structured so their symmetric or directional effects on performance could be predicted. Most recently, a new perturbation approximation approach was utilized to estimate the impact of well-structured MSF errors on the optical performance metrics like Strehl ratio and MTF [25, 26]. In this dissertation, we consider MSF errors to be quasi-structured, meaning the errors contain structured characteristics but with some variations and anisotropy like those seen in real measurements.

The second category includes studies related to specification of MSF errors. Additional recent works consider the linear structure function [27-29] and the area structure function [30-32]. While the linear structure function does not reflect the level of isotropy of surface errors, the shapes of these errors are reflected within the area structure function. Studies on how to extract the isotropy information from an area structure function could be a topic of future research. Most recently Zernike polynomials [33-35] and Q-type Forbes polynomials [2, 36] have been utilized for specification and impact of MSF errors. The orthogonal properties of Zernike polynomials along with linear systems theory of MTF provide a tool to separate performance degradation caused by different MSF errors. However, in cases where a large number of Zernike polynomials are needed to specify an

MSF error, numerical limitations could undermine this orthogonality. Thus, Zernike polynomials could play an essential role on tolerancing the impact of MSF errors on freeform surfaces, which are most often designed using Zernike polynomials. In this case, the low PV and semi-random surface residuals after a good Zernike fit need to be treated separately by scattering theory and statistical approaches.

The third main category related to MSF studies is concerned with mitigation strategies [37-39]. For instance, studies show that random tool path generation can lead to more isotropic surfaces [37]. The effort to randomize machine tool paths has been primarily limited to the most demanding applications, such as lithography. While randomizing the tool path and the tool tip itself may be needed for some applications, finding a balance between fabrication costs and required surface quality are important.

1.2 Approach and organization of this document

It is valuable to develop mitigation strategies to minimize MSF errors during the fabrication process while not dramatically increasing costs by over-specifying the surface. In article one [40] (Chapter 2), performance-driven predictive models are developed to help manufacturers determine nominal fabrication parameters for diamond machined optics based on a targeted optical performance. These models can estimate the impact of diamond tool signatures on the optical performance of a part. The results of this semi-empirical study agree very closely with results predicted by perturbation approximation methods [25].

To truly understand the impacts of MSF errors on optical performance, it is important to use a performance metric that can capture the impacts of the structured and anisotropic nature of these errors on both illumination and spatial resolution, independent of

orientation. The MTF in its complete 2D form contains this information, but the conventional 1D format does not. Historically, optical systems have been primarily symmetrical, and thus how to utilize the information within a complex and asymmetric 2D MTF has not been deeply considered. In article two [41] (Chapter 3), we propose a new MTF analysis approach that captures key information within a 2D MTF and summarizes it in the more familiar 1D format in a practical and user-friendly way. This outcome facilitates effective characterization of the impacts of anisotropic MSF errors on optical performance.

To effectively quantify MSF errors on a part, a surface specification should capture magnitude, spatial frequency and a measure of the surface anisotropy. This is important to enable the testing process. Widely used surface specification methods, such as Power Spectral Density (PSD), Linear Structure Function, bandlimited RMS, and RMS slope are discussed below. Experience indicates various situations where a part specified with these methods have met the required specifications but have not had the expected optical performance. Therefore, in article three [42] (Chapter 4), a new specification method is introduced which is able to capture the magnitude and anisotropy of MSF errors at the same time. This new surface specification builds on the approach developed in article two and has a strong connection with MTF as an optical performance metric. Tools for characterization of the impact on anisotropic MSF errors on optical performance (article two) plus an effective surface specification for MSF errors (article three) are key requirements to enable testing and tolerancing these errors.

In the following, we summarize key optical performance and surface metrology definitions that are needed to place the results of the three articles in the proper context.

1.3 Optical performance metrics

1.3.1 Point Spread Function (PSF)

The point spread function (PSF) of an optical system is the image of a point source. The coherent PSF of a linear and shift invariant coherent imaging system is the Fraunhofer diffraction [43, 44] integral of the pupil function P(ξ,η):

$$h_c(x,y) = \frac{A}{\lambda z_i} \iint P(\xi,\eta) e^{-i\frac{2\pi}{\lambda z_i}(\xi x + \eta y)} d\xi\, d\eta, \tag{1.1}$$

For incoherent imaging, fields at any two points in the object are completely uncorrelated, and therefore each imaged point adds in intensity rather than amplitude. Thus, the incoherent point spread function is the squared modulus of the coherent point spread function [44].

$$h_i(x,y) = |h_c(x,y)|^2 = \left| \frac{A}{\lambda z_i} \iint P(\xi,\eta) e^{-i\frac{2\pi}{\lambda z_i}(\xi x + \eta y)} d\xi\, d\eta \right|^2. \tag{1.2}$$

1.3.2 Strehl Ratio (SR)

The Strehl ratio (SR) is a commonly used, single-number performance metric. SR is defined as the ratio of on-axis intensity at the image plane for an aberrated system to that of a diffraction limited system [45]. For small wavefront aberrations and therefore small wavefront variances (σ_ϕ^2), the SR can be calculated using the Maréchal approximation [46]:

$$SR \approx \exp(-\sigma_\phi^2). \tag{1.3}$$

where:

$$\sigma_\phi^2 \cong -\left(\frac{2\pi}{\lambda}\right)^2 (\Delta n)^2 \sigma^2, \qquad (1.4)$$

Where σ^2 is the variance of the surface error taken over the clear aperture, σ is the RMS surface error, λ is the wavelength, and Δn is the difference between the refractive indices of the surface and the surrounding medium [14]. This approximation provides a means of estimating a system's performance based solely on the wavefront variance [47] and thus of the surface RMS error. Since by definition the wavefront variance and surface RMS error are not sensitive to the shape of distribution of data over their spatial frequency content, the SR is not able to distinguish between two wavefront variances with the same values but different shapes [48].

1.3.3 Encircled Energy

The energy distribution on the focal plane is given by:

$$E(x,y) = \iint PSF(\xi,\eta) f(x-\xi, y-\eta) d\xi d\eta, \qquad (1.5)$$

which is the convolution of the point spread function and the geometric image of the object. Thus, the encircled energy (EE) can be obtained from:

$$EE = \frac{\displaystyle\iint_{x^2+y^2<r^2} E(x,y)dxdy}{\displaystyle\iint E(x,y)dxdy}, \qquad (1.6)$$

where r is the distance in the focal plane from the optical axis [49]. In another format, the encircled energy radius (EER) could be defined as the radius of a circle in the focal plane from the optical axis that contains certain amount of energy (e.g. 83% of PSF energy).

Similar to Strehl ratio, EE or EER are single numbers that do not reflect the impact of anisotropy on optical performance.

1.3.4 Modulation Transfer Function (MTF)

The modulation transfer function (MTF) is the magnitude response of the optical system to sinusoids of different spatial frequencies [45]. In Fourier optics [43], MTF can be defined as the magnitude of the Fourier transform of the point spread function (PSF):

$$MTF(f_x, f_y) = \left| \int\int_{-\infty}^{\infty} PSF(x,y) e^{-j2\pi(xf_x + yf_y)} dxdy \right|, \tag{1.7}$$

Where f_x and f_y denote the spatial frequencies associated with the x and y spatial variables [43].

Since a 2D MTF is complex and less convenient as a practical tool, MTF specifications are generally given to manufacturers based on the conventional 1D-MTF representation, which plots a specific cross-section or cross-sections of the 2D MTF. However, a cross section is an incomplete specification if the performance of a system is not rotationally symmetric, or if the MTF is not a separable function of x and y spatial frequencies. An easy-to-use means to specify performance that guarantees that the required performance is met regardless of the orientation of spatial frequencies in the image is very desirable. To this end, in this dissertation (article two) we propose a performance specification approach

that captures key information from the 2D MTF and presents it in the more familiar 1D format [41, 50].

1.4 Surface specification methods

1.4.1 Power Spectral Density (PSD)

Power spectral density (PSD) is a powerful method for surface specification. In optics, PSD has been used for specifying high-frequency surface errors to predict scattering properties of a surface [51-55], and more recently has been applied to quantify the full spectrum of surface errors [56, 57]. The PSD provides an effective tool to filter measurement data based on the spatial frequency range of interest. This approach has been utilized within commercial surface metrology software packages [58].

The PSD is computed from the amplitude of spatial frequency components present in the Fourier spectrum of the surface height of an optical component, and is intrinsically a two-dimensional function. For any real-world case, the Fourier transformation is approximated as a discrete transform. In summary, the two-dimensional discrete PSD expression can be written as:

$$H(u,v) = \sum_{n_x=0}^{n_x-1} \sum_{n_y=0}^{n_y-1} h(x,y) e^{-2\pi j(ux/n_x + vy/n_y)} = \Im\{h(x,y)\}, \qquad (1.8)$$

$$PSD(u,v) = \frac{\Delta x \, \Delta y}{n_x \, n_y} |H(u,v)|^2, \qquad (1.9)$$

Where $H(u,v)$ is the discrete Fourier transform of a surface height map $h(x,y)$, x and y are the surface position variables, n_x and n_y are the total number of sample points in each domain respectively, u and v are the corresponding spatial frequency variables, and the $\Im$

symbol in Eq. (1.5) represents a two-dimensional fast Fourier transform (FFT) routine [59, 60]. As we can see from Eq. (1.6), the PSD has units of (length)^2(length)^2, which for example would be (nm)^2(mm)^2 if we choose the height units in nm and the lateral units in mm. The ISO 10110-8 specification provides drawings based on 1D PSD specification [61]. The 1D PSD could be a cross section of 2D PSD or an average.

1.4.2 Bandlimited RMS

The bandlimited root-mean-square (RMS) of surface error heights is widely used within the metrology, manufacturing, and optical design communities [14, 61]. It is typical to utilize the PSD to compute the RMS error for given spatial frequency bands. The bandlimited RMS error is the volume underneath the 2D-PSD surface within the given band, and can be computed through Eq. (1.10) for discreet sets of data:

$$RMS = \sqrt{\sum_{n_{v\,low}}^{n_{v\,high}} \sum_{n_{u\,low}}^{n_{u\,high}} PSD(u,v)\,\Delta u\,\Delta v} \; , \qquad (1.10)$$

Where n_u and n_v denote the index of frequency arrays in the *u* and *v* directions, respectively. Another way to calculate a bandlimited RMS for a surface is to first apply a spatial filter on the surface data and then simply calculate the root mean square of the errors on the surface. *Note that the RMS calculation is not sensitive to the shape of distribution of errors on the surface.* This could result in underestimating the impact of anisotropic surface errors on optical performance. The ISO 10110 specification (Optics and photonics – Preparation of drawings for optical elements and systems) provides drawings based on RMS waviness specification [61].

1.4.3 Surface Slope

Most optical element drawings and specifications control the amplitude of the surface form error (the optical surface figure error) by setting a maximum limit on the peak to valley (PV) or RMS departure of the surface from the mathematically perfect form. The rate of change of that surface figure error can also be an important parameter that the optical designer should be concerned with in order to ensure that the final performance of the system meets requirements. Unfortunately, there seems to be an absence of any widely distributed and accepted standard for specifying surface slope errors [62].

Despite the choice of algorithm for slope calculation, the slope magnitude is a single number, overall magnitude of slope X added to slope Y:

$$Slope\ mag = \sqrt{Slope\ X + Slope\ Y}, \qquad\qquad (1.11)$$

and thus, may not be able to distinguish between surfaces with different anisotropy.

1.5 Other considerations

The following three articles [40-42], covering Chapter 2-4, are fruits of a broader research effort. The impacts of surface errors on optical performance were studied and evaluated by incorporating surface topography data and creating custom codes in MATLAB. In Chapter 2 [40], predictive models are developed by a semi-empirical approach that relies on these simulation capabilities to study the impact of MSF errors.

To find a practical way to characterize the impact of MSF errors on the optical performance, the Modulation Transfer Function (MTF), average MTF drop, Strehl ratio, encircled energy, and Point Spread Function (PSF) were analyzed as optical performance

metrics for various optical systems. The 2D MTF was shown to be the most promising metric for observing the impact of MSF errors; in Chapter 3 [41] we develop means to extract the key information from a 2D MTF for performance characterization purposes.

Zygo's Mx software was used to analyze measurement data and MATLAB was used for data processing/conversions. Different commonly used surface specification methods, such as PSD, RMS, Slope, Linear structure function, were studied and applied to different surfaces to see what is lacking and to better understand the root of problems in MSF specification. ISO 10110-8 was also investigated [48] to understand the specification trend for MSF errors before developing a new surface specification in Chapter 4 [42].

CHAPTER 2: PREDICTIVE MODELS FOR THE STREHL RATIO OF DIAMOND-MACHINED OPTICS [40]

2.1 Abstract

This paper provides a practical connection between the Strehl ratio as an optical performance metric and manufacturing parameters for diamond machined optics. The choice of fabrication parameters impacts residual mid-spatial frequency groove structures over the part's surface, which reduce optical performance. Connections between the Strehl ratio and the fabrication parameters are studied using rigorous Rayleigh-Sommerfeld simulations for a sample optical system. The connections are generalized by incorporating the shape of diamond-machined groove structures and the effects of optical path differences for both transmissive and reflective optics. This work validates the analytical representation of the Strehl ratio as a Fourier transform of a probability density that relates to surface errors. The result is a practical tool that can be used to guide the choice of machining parameters to achieve a targeted optical performance.

2.2 Introduction

The development of computer-controlled sub-aperture fabrication techniques has opened new perspectives to the future of optics as well as new challenges [1-2]. Aspheric and freeform surfaces fabricated with such deterministic turning, milling, grinding, and polishing methods leave structured mid-spatial frequency (MSF) surface errors with 'signatures' that can be identified with the specific fabrication processes [3-4]. Studies show that MSF errors can cause image artifacts and otherwise degrade optical performance

[5-8]. In this paper, we address surface errors resulting from diamond machining processes, which appear primarily as cusp-shaped grating-like patterns as shown in Fig. 2-1.
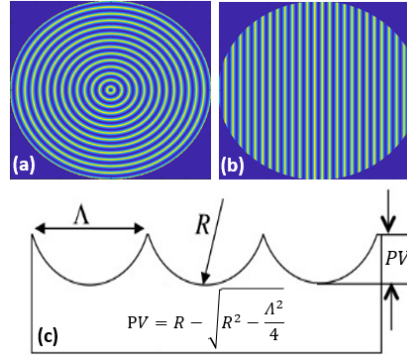

Figure 2-1: Primary MSF residuals resulting from (a) diamond turning, (b) diamond raster milling, (c) Cross section of the assumed MSF residuals. Λ represents the spacing between groove structures, R is radius of the diamond tool tip, and PV is the peak to valley of the residual surface structure.

The specification of MSF errors on optical surfaces is sometimes overlooked by optical designers. This is partially due to limitations of commonly-used surface specs for these types of errors [9], and partially because the impacts of MSF errors on optical performance are often underestimated or not well understood. Such errors can cause confusion between designers and manufacturers when a part does not perform as expected, even though it meets the requested surface specifications [10]. Therefore, to avoid poor performance, optical surfaces are often over-specified, which unnecessarily adds to manufacturing cycle times and costs. This motivates the present work, which uses a semi-empirical approach to connect the Strehl ratio (SR) directly to fabrication parameters for well-structured MSF errors from diamond machining processes.

A recent theoretical approach [11-12] expressed the SR and the Optical Transfer Function (OTF) in terms of the Fourier transform of a probability density that is related to the statistics of the MSF structures. For the cases of diamond turned or milled surfaces, the

circular cusps typically left behind are approximated as parabolic segments in order to attain an analytic expression for the SR, which can be written as:

$$SR = \frac{\pi}{4\phi} \left\| erf \left| (1+i)\sqrt{\frac{\phi}{2}} \right| \right\|^2 .$$

(2.1)

Here ∅ is the maximum optical phase difference resulting from the groove structures, and *erf* is the error function. This analytic expression is useful for further theoretical analysis; the goal in these prior works was to provide intuition on the behavior of the SR. In contrast, in this paper we provide prescriptive rules of thumb for optical manufacturers to optimize fabrication parameters based on SR. The semi-empirical approach proposed here also demonstrates a useful method to establish connections for additional surface error types that are difficult to describe analytically, providing a baseline for further work in this area. We now discuss a semi-empirical approach for connecting the SR to fabrication parameters for diamond machined optics.

2.3 Model and Approach

As a first step towards understanding behavioral changes in the SR with respect to fabrication parameters, we solve the problem for a case-specific situation. We developed a MATLAB™ toolbox with three main operations: (1) Synthesizing a lens model with desired form; (2) synthesizing a MSF texture (from either turning or milling) based on the input fabrication parameters and adding it to the surface of the lens; and (3) calculating the Point Spread Function (PSF), OTF, and the SR of the resulting composite structure using rigorous Rayleigh-Sommerfeld simulations (RSS), The SR is defined as [13]:

$$SR \equiv \frac{\iint OTF\left(f_x, f_y\right) df_x df_y}{\iint OTF_{perfect}\left(f_x, f_y\right) df_x df_y}. \tag{2.2}$$

Toolbox calculations were tested and compared to Rayleigh-Sommerfeld-based simulations within VirtualLab™ with excellent agreement. Standardized results are obtained by evaluating the performance of a diffraction-limited optic (prior to adding MSF errors) located at the aperture stop, similar to performance evaluation assumptions within Zygo's Mx™ software.

This toolbox enables us to assess changes in optical performance with respect to fabrication parameters. Our goal is to find general connections for reflective or transmissive optics for any wavelength or material without the need for more rigorous simulations. To this end, we first explore a specific case and then generalize the results.

In the case study, we assume a 4 mm diameter f/25 PMMA (n = 1.4934) lens at the pupil with plane wave illumination at λ = 532 nm. The diamond tool's tip radius, R, is set to 1 mm in this example. The machining feed per revolution (for diamond turning) or step-over (for diamond raster milling), collectively represented as Λ, is kept variable. A pixel size of δx = 0.3 μm was used for the RSS to enable SR values accurate to three decimal points. Fig. 2-2 compares the simulation results of the SR versus Λ for both diamond-milled and diamond-turned surfaces. As we will discuss later in the paper, the difference between the performance of diamond-milled and diamond-turned surfaces are not reflected in SR simulations.
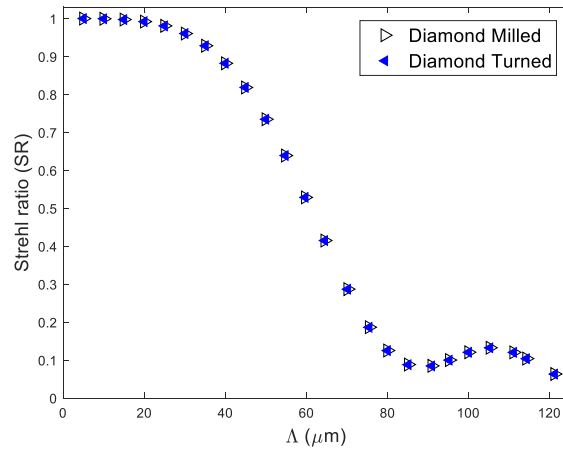
Figure 2-2: The impact of diamond machined MSF errors on the SR with respect to groove spacing for the specific case study. Simulation results indicate similar SR values for diamond-milled and diamond-turned optics (RMSE=0.000172).

From a manufacturing perspective, increasing Λ is desirable as doing so reduces the required manufacturing time and cost. However, as expected, Figure 2-2 shows that increasing Λ leads to a lower SR. In practice, Λ is normally chosen to be small enough to meet a required root mean square (RMS) surface deviation that guarantees the smooth surface requirements.

We now generalize our results. Surface imperfections create wavefront distortions since an unwanted surface height leads to an undesired optical phase difference. An optical path difference of one wavelength, λ results in a phase difference of 2π. Therefore, for a surface height of $h(x,y)$, the optical phase difference $\phi(x,y)$ equals:

$$\phi(x,y) = kAh(x,y), \qquad\qquad (2.3)$$

where $k=2\pi/\lambda$, $A = n_s-n_0$ (in transmission) or $2n_0$ (in reflection), with n_s being the refractive index of a transmissive material, and n_0 the ambient refractive index.

For diamond machined surfaces, it is straightforward to determine the relationship between the peak-to-valley (PV) of the residuals and the machining parameters:

$$PV = R-\sqrt{R^2 - \frac{\Lambda^2}{4}} = R - R\left[1 - \frac{\Lambda^2}{8R^2} + \frac{\Lambda^4}{128R^4} - \dots\right] \approx \frac{\Lambda^2}{8R}, \tag{2.4}$$

where the approximation using the Taylor series expansion is valid for $R \gg \Lambda$. It is obvious that an increase in groove spacing results in a surface error with larger PV, which imparts a larger optical phase difference on the incident wavefront and lowers the SR, as seen in Fig. 2-2. By substituting PV, in Eq. (2.4), for h = PV/cosθ_i, where θ_i is the incident angle, we calculate the maximum optical phase difference imparted on the wavefront to be:

$$\phi = \frac{kA}{\cos\theta_i}\left(R - \sqrt{R^2 - \frac{\Lambda^2}{4}}\right) \approx \frac{kA\Lambda^2}{8R\cos\theta_i}. \tag{2.5}$$

Equation (5), although conceptually intuitive, is an important outcome that enables a connection between the manufacturing parameters and optical performance. We note that the coordinate-dependent height function, $h(x,y)$, has been replaced with a constant PV. This is justified since the diamond cusp surface shape is implicitly contained within the optical performance simulations shown in Fig. 2-2.

Next, we substitute the application parameters used in the case-specific example of Fig. 2-2 into Eq. (2.5), with no approximation, and perform a Gaussian fit [14] over the new data set to obtain Eq. (2.6), which gives a general relation between the SR and ϕ for diamond-machined surfaces:

$$SR \approx \exp\left[-\left(\frac{\phi}{3.24}\right)^2\right]. \qquad (2.6)$$

We note from Fig. 2-3 that the fit is excellent for $\phi < 4.7$ *rad* with a Root Mean Square Error (RMSE) of 0.0036. We assert that this limit is sufficient for practical purposes since larger errors correspond to rough surfaces which fail basic RMS surface requirements and $SR < 0.125$. However, higher-order polynomial fits can be performed for larger values of ϕ if required. Figure 2-3 shows the resulting plot of the SR vs ϕ.
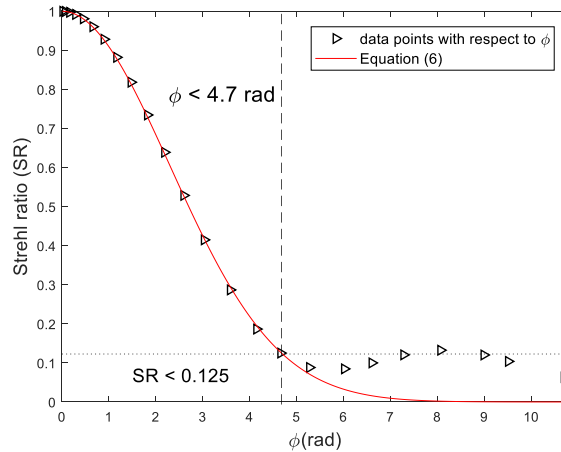

Figure 2-3: SR versus optical phase difference ϕ. The red curve represents Eq. (2.6).

To provide a predictive tool we must invert Eq. (2.6):

$$\phi \approx 3.24\sqrt{-\log_e(SR)}. \qquad\qquad (2.7)$$

This expression presents ϕ as a function of SR. Equation (2.7) provides a useful predictive tool for designers to quantify required surface specifications and for manufacturers to guide the choice of machining parameters based on the target SR.

We now present three example applications of the semi-empirical models. We note that SR values are given to several decimal places only to enable comparison of the model results.

Example 1: Predicting the SR from machining parameters for a lens. Consider a 5 mm diameter f/10 focusing element made of Germanium (n = 4.0242) for use at λ = 4µm. The lens is diamond-turned with Λ = 50µm and R = 1.5 mm. Table 2-1 compares the on-axis prediction with simulation results.

Table 2-1. Predicted SR versus Simulated SR for Example 1.

Λ (µm)	R (mm)	ϕ (rad)	SR Predicted	SR RSS	Δ
50	1.5	0.990	0.910	0.914	0.004

As you can see from table 1, after simulating the performance ($\delta x = 0.3$ µm) and calculating the SR, $\Delta = |SR_{RSS} - SR_{Predicted}|$ is negligible. Therefore, Eq. (2.6) predicts SR without the need for more rigorous simulations.

Example 2: Predicting the SR from machining parameters for a mirror. Assume a 3mm diameter f/15 focusing mirror operating at λ = 480 nm. The mirror is diamond-milled with Λ = 25

μm and R = 1 mm. In Table 2-2, we compare the predicted SR with the Rayleigh-Sommerfeld simulated SR (δx = 0.3 μm) for three different field angles.

Table 2-2. Predicted SR vs simulated SR for different field angles.

θ_i (degrees)	ϕ (rad)	SR $_{Predicted}$	SR $_{RSS}$	Δ
0	2.05	0.670	0.669	0.001
21	2.19	0.633	0.630	0.003
30	2.36	0.588	0.583	0.005

In Table 2-2, predicted results are in excellent agreement with more rigorous, time consuming simulations for all field angles with negligible differences.

Example 3: Determination of machining parameters for a required SR value. Consider an 8mm diameter f/5 diamond-turned PMMA (n = 1.4883) lens working at λ = 650 nm. Assuming a diamond tool with R = 0.5 mm, we would like to find the maximum groove spacing *Λ* that results in an optic with on-axis SR = 0.9. Solving Eq. (2.7) for SR=0.9 gives the maximum permitted optical phase difference of ϕ = 1.05 *rad*. Substituting this value into Eq. (2.5) predicts Λ ~ 29.82 μm. To facilitate the performance simulation of this optic within MATLAB™, we slightly modify Λ to 29.85 μm to generate an integer number of cusp errors per aperture and reduced the simulation resolution from δx = 0.3 μm to δx = 0.6 μm overcome computational challenges. PSF and SR simulations confirm the accuracy of the semi-empirical model with simulated *SR* = 0.899 ~ 0.9. In practice, the groove spacing could be rounded downward slightly (for example, to 29 μm) to provide additional performance margin and to simplify manufacturing setup.

2.4 Discussion

The presented models can be used as tools to guide both the quantification of MSF surface specifications by optical designers and the choice of diamond machining parameters by manufacturers. As discussed previously, determination of the maximum groove spacing Λ for a given tool radius R that will still provide the required optical performance is desirable, as doing so reduces required manufacturing cycle time and cost.

For example, in diamond turning the groove spacing is determined by both the rotation rate of the machining spindle and the velocity (feed rate) of the diamond tool orthogonal to the axis of rotation. The resulting feed per revolution is then given by [4]:

$$\Lambda = \frac{Feed\,(mm/\min)}{Spindle\,Speed\,(rev/\min)}. \tag{2.8}$$

Table 2-3 illustrates a range of representative manufacturing parameters for diamond-turning the lens in Example 3 compared to a mirror with the same f/# and application parameters. The approximation in Eq. (2.5) helps to simplify these types of calculations. The differences in parameters for the lens and 'equivalent' mirror result from the optical phase differences between the transmissive and reflective cases. Note that we have rounded the groove spacing down to the nearest integer value, which simplifies manufacturing setup and provides additional performance margin.

Table 2-3. Sample manufacturing parameters for Example 3.

	SR	Λ_{Lens} (µm)	Λ_{Mirror} (µm)	R (mm)	Spindle (rpm)	Feed$_{Lens}$ (mm/min)	Feed$_{Mirror}$ (mm/min)
I	0.9	51	25	1.5	1500	76.5	37.5
II	0.9	47	23	1.25	1750	82.25	40.25
III	0.9	42	20	1	2000	84	40
IV	0.9	29	14	0.5	1000	29	14
V	0.9	29	14	0.5	2000	58	28

We note that there are other sources of MSF errors that occur in diamond-machined optical surfaces besides the 'cusp' shapes that we have considered, including, for example, asynchronous error motions, external and self-induced vibration, thermal drift, materials effects, and so on. [4, 15-18]. These additional error sources are also connected to the feed rate and spindle speed. With the guidance of the presented models, a manufacturer can use their expertise to select the best combination of tool radius, feed rate, and spindle speed that gives the required result at minimal time and cost while also minimizing other sources of error.

The use and limitations of the SR as an optical performance metric for diamond machined optics is worthy of additional consideration. Fig. 2-2 suggests that the optical performance of diamond-turned and diamond-milled components with equivalent groove spacing Λ will be quite similar. While this is generally true for very high-quality optics, the performances of turned and milled components deviate as the groove spacing increases due to the difference in symmetry of the residual surface structures [10, 12]. For such cases, other performance measurements, such as a 2D Modulation Transfer Function (MTF), would represent optical performance more effectively than

the SR. Such relationships and performance metrics are currently being studied and will be considered in more detail in future publications.

Figure 2-4 compares the semi-empirical model of Eq. (2.6) with the analytic model of Eq. (2.1) and a 5th order polynomial fit over the full range of ϕ values. This figure shows that the semi-empirical approach developed in this paper agrees very well with the analytic model based on prior work [11-12]. The close agreement supports the validity of both approaches. However, Eq. (2.6) is designed to be more succinct, user-friendly and invertible to Eq. (2.7) to enable a predictive model for both manufacturer and designer, which is not the case with Eq. (2.1).
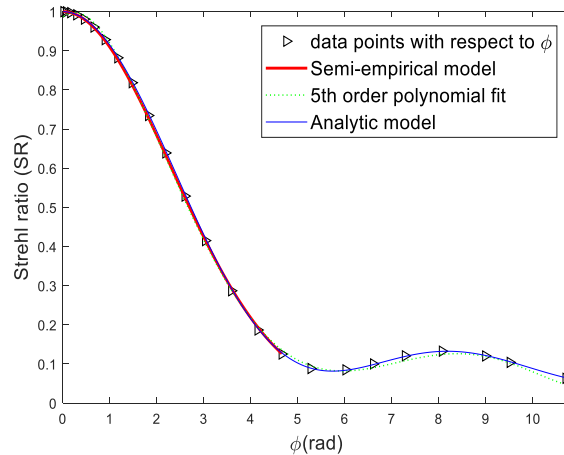
Figure 2-4: Comparison of the semi-empirical and analytic SR expressions, given by Eq. (2.6) and (2.1), respectively. For $\phi < 4.7\ rad$, the two models differ by a RMSE of 0.0058.

2.5 References

1. D. M. Aikens, J. E. DeGroote, and R. N. Youngworth, "Specification and Control of Mid-Spatial Frequency Wavefront Errors in Optical Systems," in Frontiers in Optics 2008/Laser Science XXIV/Plasmonics and Metamaterials/Optical Fabrication and Testing, OSA Technical Digest (CD) (Optical Society of America, 2008), paper OTuA1.

2. G. W. Forbes, "Never-ending struggles with mid-spatial frequencies", Proc. of SPIE Vol. 9525, 95251B (2015)·

3. C. R. Dunn and D. D. Walker, "Pseudo-random tool paths for CNC sub-aperture polishing and other applications," Opt. Express 16, 18942-18949 (2008).

4. M. Bass, C. DeCusatis, J. Enoch, V. Lakshminarayanan, G. Li, C. Macdonald, V. Mahajan, and E. V. Stryland. *Handbook of Optics, Third Edition Volume II: Design, Fabrication and Testing, Sources and Detectors, Radiometry and Photometry*. (McGraw-Hill, 2009), Chap. 10.

5. J. A. Shultz, M. Davies, and T. J. Suleski, "Effects of MSF errors on performance of freeform optics: Comparison of diamond turning and diamond milling," in Imaging and Applied Optics 2015, OSA Technical Digest (online) (Optical Society of America, 2015), paper FT4B.3.

6. J. M. Tamkin, W. J. Dallas, and T. D. Milster, "Theory of point-spread function artifacts due to structured mid-spatial frequency surface errors", App. Opt., 49, No. 25, 4814-4824 (2010).

7. J. M. Tamkin, T. D. Milster, and W. J. Dallas, "Theory of modulation transfer function artifacts due to mid-spatial-frequency errors and its application to optical tolerancing," Appl. Opt. 49, 4825-4835 (2010).

8. J. Filhaber, "Mid-spatial-frequency errors: the hidden culprit of poor optical performance", Laser Focus World 49(8), p. 32 (2013).

9. Z. Hosseinimakarem, H. Aryan, A. Davies, and C. Evans, "Considering a Zernike polynomial representation for spatial frequency content of optical surfaces," in Imaging

and Applied Optics 2015, OSA Technical Digest (online) (Optical Society of America, 2015), paper FT2B.2.

10. H. Aryan, C. J. Evans, and T. J. Suleski, "On the Use of ISO 10110-8 for Specification of Optical Surfaces with Mid-Spatial Frequency Errors," in Optical Design and Fabrication 2017 (Freeform, IODC, OFT), OSA Technical Digest (online) (Optical Society of America, 2017), paper OW4B.2.

11. M. A. Alonso and G. W. Forbes, "Strehl ratio as the Fourier transform of a probability density of error differences," Opt. Lett. 41, 3735-3738 (2016).

12. K. Liang and M. A. Alonso, "Understanding the effects of groove structures on the MTF," Opt. Express 25, 18827-18841 (2017).

13. J.W. Goodman, *Introduction to Fourier Optics* (Roberts and Company, 2005).

14. MathWorks, Fitting Toolbox: User's Guide (R2017b).

15. S. Rakuff and P. Beaudet, Opt. Eng. 46(10) 103401 (2007).

16. K. Cheng (eds), *Machining Dynamics* (Springer, 2009), Chap. 9.

17. A. Sohn, L. Lamonds, and K. Garrard, "Modeling of Vibration in Single-Point Diamond Turning," Proceedings of the ASPE, American Society of Precision Engineering, no. 21st Annual Meeting, pp. 15-20 (2006).

18. J. A. Shultz, H. Aryan, J.D. Owen, M.A. Davies, and T.J. Suleski, "Impacts of sub-aperture manufacturing techniques on the performance of freeform optics", Proceedings ASPE/ASPEN Spring Topical Meeting: Manufacture and Metrology of Structured and Freeform Surfaces for Functional Applications, Paper 0061, p. 29 (2017).

CHAPTER 3: THE MINIMUM MODULATION CURVE AS A TOOL FOR
SPECIFYING OPTICAL PEROFRMANCE: APPLICATION TO SURFACES WITH
MID-SPATIAL FREQUENCY ERRORS [41]

3.1 Abstract

There are a variety of common situations in which specification of a one-dimensional modulation transfer function (MTF) or two orthogonal profiles of the 2D MTF are not adequate descriptions of the image quality performance of an optical system. These include systems with an asymmetric on-axis impulse response, systems with off-axis aberrations, systems with surfaces that include mid-spatial frequency errors, and freeform systems. In this paper, we develop the concept of the Minimum Modulation Curve (MMC). Starting with the two-dimensional MTF in polar form, the minimum MTF for any azimuth angle is plotted as a function of the radial spatial frequency. This can be presented in a familiar form similar to an MTF curve and is useful in the context of guaranteeing that a given MTF specification is met for any possible orientation of spatial frequencies in the image. In this way, an MMC may be of value in specifying the required performance of an optical system. We illustrate application of the MMC using profile data for surfaces with mid-spatial frequency errors.

3.2 Introduction

The MTF is a measure of system performance over its full spatial frequency range. The MTF provides an objective evaluation of a system's imaging contrast and is expressed as the ratio of contrast in the image to contrast in the object as a function of spatial frequency [1]. MTF specifications given to manufacturers are often based conceptually on the

conventional 1D-MTF representation, which plots a particular cross section of the 2D MTF, since the 2D MTF is less convenient as a practical specification. However, plotting a cross section is an incomplete specification of performance if the system's MTF is not rotationally symmetric or if the MTF is not a separable function of x and y spatial frequencies. A means to specify performance is desirable, which would guarantee that the desired performance is met regardless of the orientation of spatial frequencies in the image. In this paper, we propose a performance specification that captures key information from the 2D-MTF and presents it in the more familiar 1D format [2].

A 2D MTF can be defined as the magnitude of the Fourier transform of the 2D point spread function (PSF):

$$MTF(f_x, f_y) = \left| \int\int_{-\infty}^{\infty} PSF(x, y) e^{-j2\pi(xf_x + yf_y)} dxdy \right|, \tag{3.1}$$

where f_x and f_y denote the spatial frequencies associated with the x and y spatial variables. The 2D MTF can be conveniently described in polar coordinates by means of the change of variables $\rho = (f_x^2 + f_y^2)^{1/2}$ and $\phi = \tan^{-1}(f_y/f_x)$, yielding $MTF(\rho, \phi)$. The radial spatial frequency ρ is represented as the radial distance from the center of the 2D polar plot and the azimuth angle ϕ corresponds to the angle measured from the f_x axis.

Section 2 introduces the concept of the Minimum Modulation Curve and its relationship to the 2D MTF. Section 3 illustrates the MMC representation with some specific examples drawn from systems with mid-spatial frequency errors, and section 4 discusses the importance of this analysis approach and possible future investigations for systems with

inherently asymmetric performance. We note that in this paper we focus on the MTF of the optical components in the system and do not consider impacts of sensors or detectors [3].

3.3 The Minimum Modulation Curve

In developing a performance specification for an optical system, it is desirable to ensure that a certain minimum MTF is present at the spatial frequencies of interest as a pass/fail criterion. Thus, we choose to determine the minimum modulation values, independent of orientation, to conform with the normal practice of setting acceptance criteria for the MTF. Choosing the minimum modulation values may be pessimistic if the MTF requirement is needed only for a specific orientation with a well-defined axis, but this is not the case for applications for which the relative orientation of the object and optical components are not well known or can vary.

Toward this end, we present the concept of the Minimum Modulation Curve (MMC), which conveniently summarizes the information contained within the 2D-MTF in the familiar form of a 1D plot, and which is suitable as a performance specification. Starting with the 2D MTF expressed in polar coordinates $MTF(\rho, \phi)$, we evaluate the MTF for all values of the azimuth angle for a given value of radial spatial frequency. The minimum MTF value at that ρ for any value of ϕ becomes the MMC value for that ρ:

$$MMC(\rho) = \min_{\phi \in [0,2\pi]} \{MTF(\rho,\phi)\}, \qquad\qquad (3.2)$$

as schematically illustrated in Fig. 3-1. The anisotropic MTF arising from a sample ZEMAX design file for a Cooke triplet with 40-degree field, at a wavelength of λ=650 nm

and off-axis field angle of 20 degrees, is used as an example. The MMC for this case is

shown in Fig. 3-2(a).
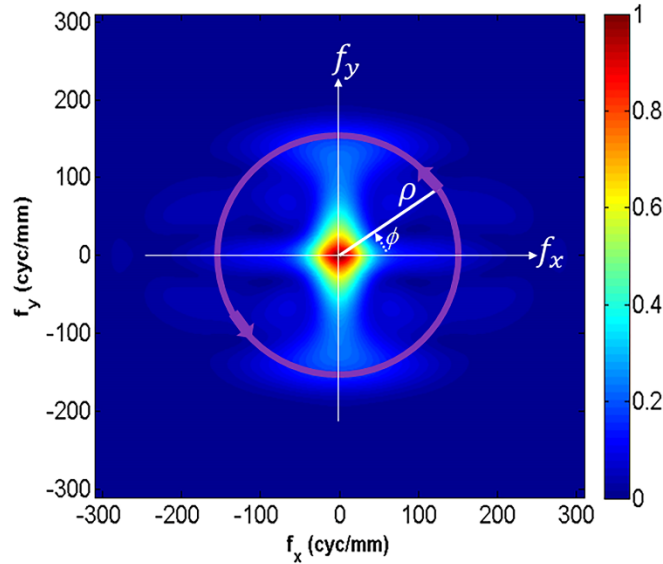
Figure 3-1: Illustrating the methodology of extracting data for each spatial frequency from a general 2D-MTF. The minimum value around each circle is extracted to generate the MMC for a given value of radial spatial frequency ρ.

It is also of interest to calculate the standard deviation of MTF values $\sigma_{MTF}(\rho)$
for each value of ρ, assuming N values of azimuth angle ϕ:

$$\sigma_{MTF}(\rho) = \sqrt{\frac{\sum\limits_{n=1}^{N}\left[MTF(\rho,\phi_n) - \dfrac{\sum\limits_{n=1}^{N}MTF(\rho,\phi_n)}{N}\right]^2}{N}}, \qquad (3.3)$$

resulting in the MTF standard deviation plot as illustrated in Fig. 3-2(b). The MMC plot

thus shows the minimum MTF for each frequency, considering all possible azimuth

directions. The 1D nature of the plot facilitates a convenient comparison of measured data

with a performance specification. In addition, the plot of MTF standard deviation $\sigma_{MTF}(\rho)$ can be used to identify the spatial frequencies that are most sensitive to anisotropy.
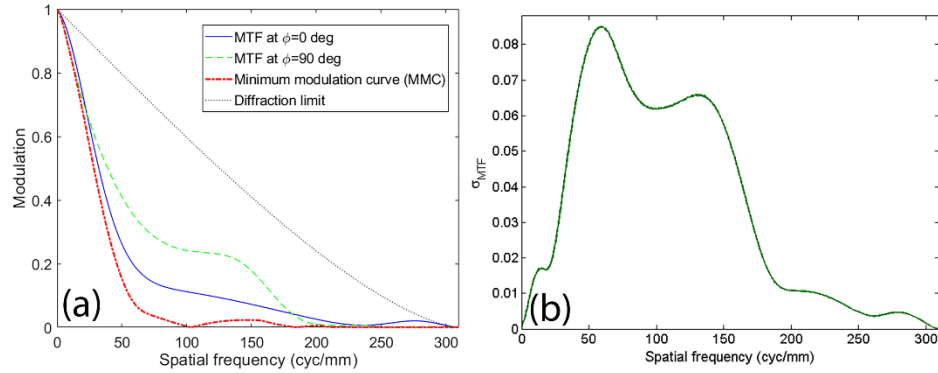

Fig. 3-2: With reference to the 2D MTF in Fig. 3-1, (a) the minimum modulation curve (dash dot red) and horizontal MTF cross section (blue), (b) MTF standard deviation at each radial spatial frequency.

With the MMC and $\sigma_{MTF}(\rho)$ thus defined, we now consider optical components with residual mid-spatial frequency surface errors to illustrate the application of this concept.

3.4 Mid-Spatial Frequency Errors and Performance Specification

Mid-spatial frequency (MSF) surface errors are common drawbacks of deterministic sub-aperture fabrication techniques [4-11]. The classic works for characterizing the impact of MSF errors on optical system performance generally assume that these errors are small and randomly distributed. Early studies on the impact of sub-aperture fabrication tool errors date back to evaluation of surface quality of diamond turned optics by Church and Zavada in 1975 [12]. However, their statistical approach requires that perturbations are small, and errors are random with no structured spatial frequencies in the Power Spectral Density (PSD) [13]. Marioge and Slansky considered the impacts of structured rotationally periodic

waviness on image quality in 1983 [14]. More recently, Tamkin [15, 16] has considered impacts of structured MSF errors on the Modulation Transfer Function (MTF). While high-spatial-frequency errors are often random in distribution and scatter the light at large angles, mid-spatial-frequency errors are far more structured and diffract the light at angles small enough to directly illuminate the image plane [17]. The distribution of this illumination depends on the structure of the errors on the surface, which in turn depends on the choice of fabrication technique. Typical MSF errors resulting from sub-aperture fabrication methods are not symmetric over the aperture, providing a suitable illustration for the presented analysis tools. It is important to keep in mind that different light distributions outside the main peak of the PSF will in result in different image quality performance. To illustrate this point, we assume two MSF errors with the same surface root mean squared (RMS) error values (82 nm) but different anisotropies. Figure 3-3 shows two diamond machined surfaces (turned and milled) synthesized in MATLAB using the same fabrication parameters: a tool-tip radius of 1 mm and $\Lambda=40$ μm, where Λ represents feed/rev for turning and step-over for milling. A sinusoidal error of 1 cycle/mm with 150 nm peak to valley was added to the resulting 'cusp-shaped' tool errors to approximate thermal drift effects from the tool chiller during manufacturing.

Grating-like sinusoidal and cusp textures, such as those in Fig. 3-3, diffract the incident light which directly affects the system's performance. We assume a 4-mm diameter f/25 PMMA (n=1.4934) lens at the aperture stop at wavelength $\lambda = 0.532$ μm and perform a Rayleigh-Sommerfeld diffraction simulation to compare the impacts of these errors on performance.
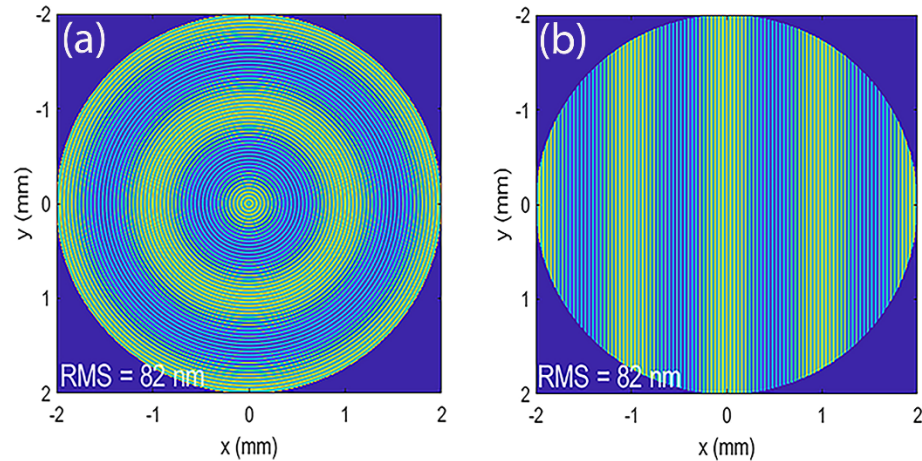
Figure 3-3: Two diamond machined surfaces with the same fabrication parameters; Diamond tool cusp errors: a tool-tip radius of 1 mm and Λ=40 µm; Sinusoidal error of 1 cycle/mm with peak to valley (PV) of 150 nm to represent thermal errors. (a) Diamond turned. (b) Diamond milled.

Figure 3-4 compares the simulated PSFs for a perfect lens with no surface errors to lenses with the errors shown in Fig. 3-1. The PSF for the perfect lens has the typical Airy disk pattern. Diffraction from the rotationally symmetric grating pattern of the turned case appears as a symmetrical irradiance distribution in rings around the main peak, while the PSF corresponding to the milled case contains localized irradiance peaks in the horizontal direction. In other words, the turned pattern diffracts the light equally in all directions while the milled pattern diffracts in the horizontal direction, parallel to the grating vector.
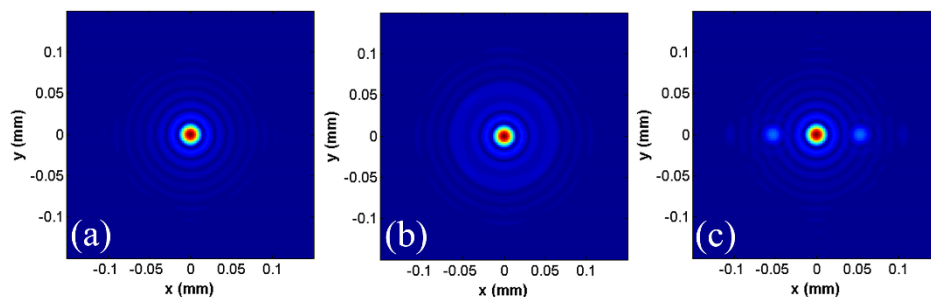

Figure 3-4: Rayleigh-Sommerfeld simulations of PSF for the above examples for the (a) perfect lens, (b) diamond turned lens, (c) diamond milled lens.

The impacts of anisotropic MSF errors on optical performance are not well-understood or well-quantified because standard characterization methods are not able to sufficiently capture these impacts. This has led to problems in surface specification and setting acceptance criteria for testing purposes as well. Any surface specification method should show connections to optical performance, and without the right performance characterization method this problem will not be solved. Therefore, it is necessary to address this issue. The Strehl ratio and encircled energy radius have previously been considered as optical performance metrics for surfaces with MSF errors. [8, 18, 19]. Therefore, we first briefly consider these two metrics with respect to anisotropic MSF errors before considering the MTF and the MMC.

Strehl ratio (*SR*) is a commonly used single-number performance metric, defined as the ratio of on-axis intensity at the image plane for an aberrated system to that of a diffraction limited system [20]. For small wavefront variances, the Maréchal approximation [21] can be used to calculate the SR as:

$$S = \exp[-(k\Delta n\, \sigma)^2],$$ (3.4)

where $k = 2\pi/\lambda$, Δn is the difference between refractive indices of the lens and the surrounding medium, and σ is the surface RMS error. Since by definition the wavefront variance and surface RMS error are not sensitive to the shape of distribution of data over their spatial frequency content, the Strehl ratio is not able to distinguish between two wavefront variances with similar values but different shapes [8, 22]. Rayleigh-Sommerfeld simulations result in *SR* = 0.8 for both cases, which agrees with prediction based on Eq.

(3.4), and illustrates the inability to distinguish between the different performance impacts of these two surface errors using Strehl ratio.

Encircled energy radius (EER) is another common performance metric, defined as the radius of a circle with a certain amount of energy (typically 83%) centered on the PSF centroid [23]. Rayleigh-Sommerfeld simulations show an 83% encircled energy radius of ~0.05 mm for both cases in Fig. 3-1. Thus, neither Strehl ratio nor encircled energy are sufficient to distinguish between the impacts of the two surface errors illustrated in Fig. 3-1.

We now make use of Eq. (3.1) to calculate the 2D MTF from the three PSFs shown in Fig. 3-4. Unlike the results discussed above for *SR* and EER, the impacts of the different MSF error symmetries from Fig. 3-1 are clearly shown by the 2D MTFs in Fig. 3-5. We note that the 2D MTF also contains the Strehl ratio information if one integrates the volume under the 2D MTF [1, 20]. Thus, the 2D MTF is a powerful tool to quantify the performance of an optical component with anisotropic performance characteristics. However, extracting key information from the 2D MTF and putting it in a one-dimensional form would make it more convenient as a means for performance specification.
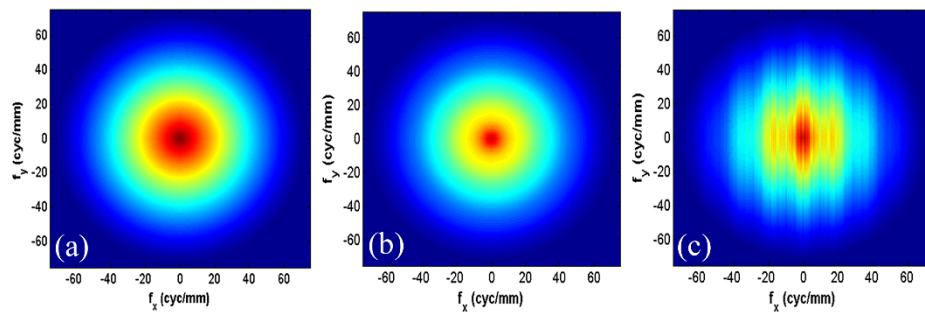

Figure 3-5: 2D-MTF simulations for the (a) perfect lens, (b) diamond turned lens, (c) diamond milled lens. Red color represents 1 and blue color represents 0 modulation in these figures.

It is common to plot 1D horizontal and/or vertical cross sections of the 2D-MTF to represent the system MTF. However, a standard cross section of MTF is not an accurate representation when the MTF lacks rotational symmetry. Figure 3-6 compares the horizontal and vertical cross section of the 2D MTF from Fig. 3-5(c). Notice that the horizontal cross section indicates many MTF oscillations while a vertical cross section is smooth and approximately diffraction limited.
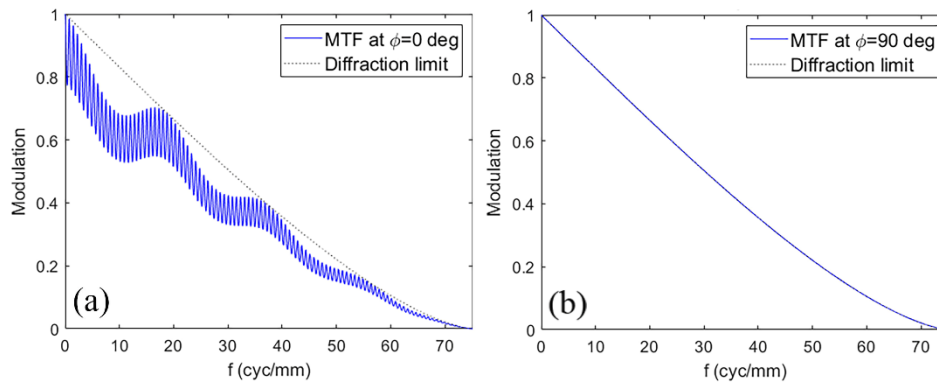
Figure 3-6: Comparing (a) horizontal and (b) vertical cross section of the 2D-MTF for the diamond milled case from Fig. 3-3(b).

The high frequency oscillations in Fig. 3-6(a) are a result of the diamond 'cusp' errors on the surface [8, 11]. In practice these oscillations will be minimal with a small machining stepover and corresponding small PV of the surface cusp error. In this example, we intentionally synthesized surfaces with a large stepover and PV to illustrate their impact in the MMC calculation.

We now apply the techniques described in Section 2 to determine the MMC and MTF standard deviation at each radial spatial frequency. The results are shown in Fig. 3-7.
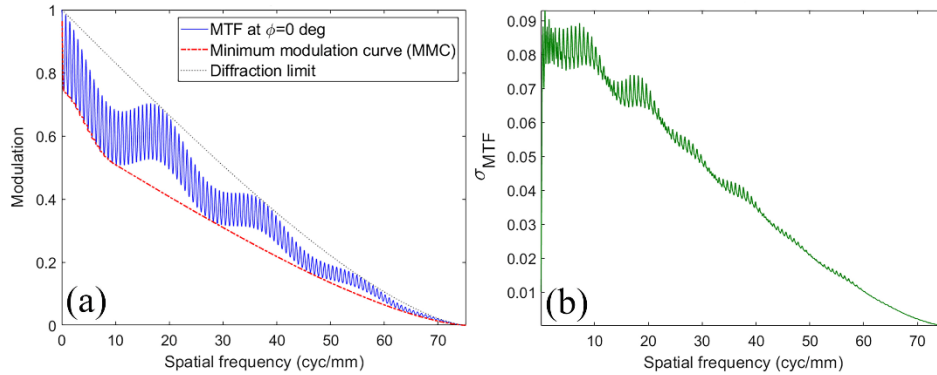
Fig. 3-7. With reference to the 2D MTF in Fig. 3-5(c), (a) the minimum modulation curve (dash dot red) and horizontal MTF cross section (solid blue), (b) MTF standard deviation at each radial spatial frequency.

We note that the MMC simplifies the oscillations on the 1D MTF in Fig. 3-7(a) by just presenting the minimum values, regardless of orientation. Also, the MTF standard deviation plot indicates that MTF varies more at low spatial frequencies, with an overall decline for higher frequencies. These tools may be useful to include in software packages for tolerancing purposes.

Rotationally asymmetric MTFs are also common when dealing with measured surface errors. As a demonstration, we consider an experimental surface error of the form shown in Fig. 3-8(a) applied to the surface of a calcium fluoride (n = 1.5576) f/10 lens in the deep ultraviolet region (λ = 157 nm). Figure 3-8(b) illustrates the 2D MTF for this system. In Fig. 3-8(c), the MMC plot indicates that, due to the anisotropy of the surface error, the actual optical performance would be worse than predicted by standard 1D-MTF cross sections. The MTF standard deviation plot in Fig. 3-8(d) shows the maximum MTF variations occur at approximately one-third of the lens cutoff frequency.
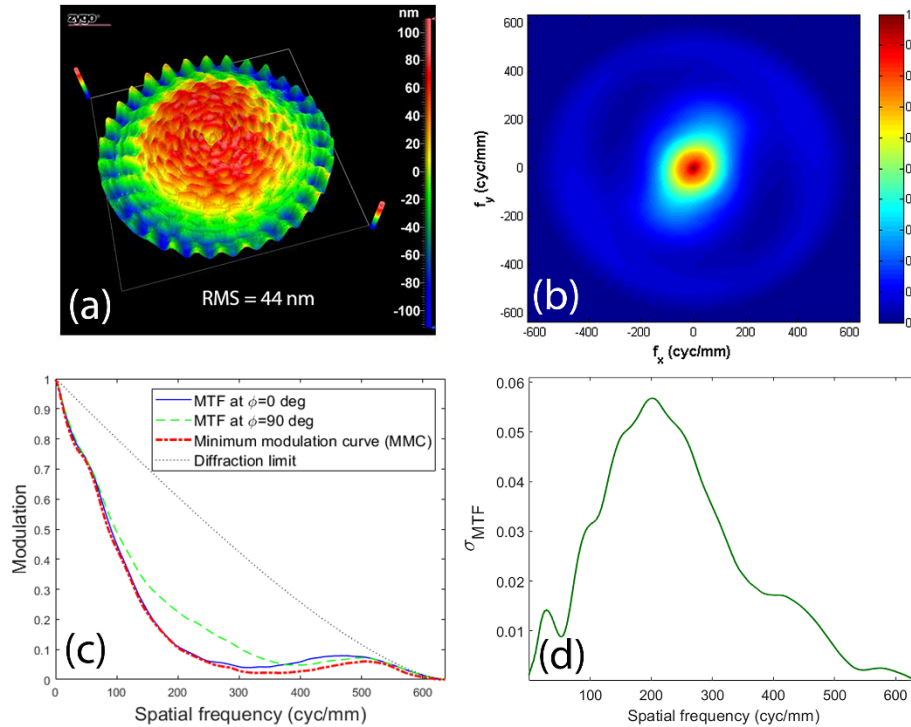
Fig. 3-8. (a) Measured surface error with RMS of 44 nm over a 127 mm clear aperture. (b) Simulated on-axis 2D MTF for a lens with this surface error. (c) Comparing MMC (dash dot red) with horizontal cross section of MTF at $\phi = 0^o$ (solid blue) and $\phi = 90^o$ (dash green). (d) MTF standard deviation at each radial spatial frequency.

3.5 Discussion and Conclusion

We have presented a new analysis approach that identifies the minimum MTF value and its standard deviation at each radial spatial frequency, which is particularly useful for characterization and specification of system performance when PSFs and MTFs are not rotationally symmetric. In particular, the MMC presents information from the 2D MTF in an intuitive 1D format. It provides a straightforward way to represent the minimum MTF as a function of radial spatial frequency, considering all directions.

While we demonstrated the MMC for optical surfaces with mid-spatial frequency errors, the concepts presented in this paper may also be useful in other situations. For instance, in

imaging applications, the final image is the weighted superposition of the system's PSF, which varies as a function of field angle, and the MTFs for off-axis field angles are often anisotropic. This is of particular importance for many modern optical systems; for instance, end users are sensitive to asymmetric image quality in digital single lens reflex (DSLR) and mirrorless camera lenses, as well as cell phone cameras [24].

Freeform optical systems also provide additional examples of PSFs and MTFs that are not rotationally symmetric. Many freeform systems have no single plane of symmetry and the performance metrics can no longer be assumed to be rotationally symmetric for such systems. Therefore, the performance evaluation must be considered over a full range of field points in two dimensions. Additionally, in augmented reality and virtual reality systems, near-eye display technology is used. In these applications, locations of the displayed image will move in response to movement of the user's head. In such situations, the user may be particularly sensitive to variations highlighted by σ_{MTF}.

3.6 References

1. J. W. Goodman, *Introduction to Fourier Optics*, (Roberts and Company, 2005).

2. H. Aryan, T. J. Suleski, "Non-directional modulation transfer function for optical surfaces with asymmetric mid-spatial frequency errors", in Optical Design and Fabrication 2019 (Freeform, OFT), OSA Technical Digest (online) (Optical Society of America, 2019), paper OT1A.2.

3. O. Hadar, A. Dogariu, and G. D. Boreman, "Angular dependence of sampling modulation transfer function," Appl. Opt. **36**, 7210-7216 (1997).

4. R. Rhorer and C. Evans, "Fabrication of optics by diamond turning," in *Handbook of Optics, Third Edition Volume II: Design, Fabrication and Testing, Sources and Detectors, Radiometry and Photometry*, M. Bass, C. DeCusatis, J. Enoch, V. Lakshminarayanan, G. Li, C. Macdonald, V. Mahajan, and E. Van Stryland, eds. (McGraw-Hill, 2009), Chap. 10.

5. W. B. Lee, C. F. Cheung, and S. To, "Materials-induced Vibration in Single Point Diamond Turning," in *Machining Dynamics,* K. Cheng, ed. (Springer, 2009), pp.263-282.

6. C. R. Dunn and D. D. Walker, "Pseudo-random tool paths for CNC sub-aperture polishing and other applications," Opt. Express **16**, 18942-18949 (2008).

7. A. Sohn, L. Lamonds, K. Garrard, "Modeling of Vibration in Single-Point Diamond Turning," Proceedings of the ASPE, American Society of Precision Engineering, 21st Annual Meeting, pp. 15-20 (2006).

8. H. Aryan, K. Liang, M. A. Alonso, and T. J. Suleski, "Predictive models for the Strehl ratio of diamond-machined optics," Appl. Opt. **58**, 3272-3276 (2019).

9. G.W. Forbes, "Never-ending struggles with mid-spatial frequencies", Proc. SPIE **9525**, 95251B (2015).

10. Z. Hosseinimakarem, H. Aryan, A. Davies, and C. Evans, "Considering a Zernike polynomial representation for spatial frequency content of optical surfaces," in Imaging and Applied Optics 2015, OSA Technical Digest (online) (Optical Society of America, 2015), paper FT2B.2.

11. J. A. Shultz, H. Aryan, J. D. Owen, M. A. Davies, and T. J. Suleski, "Impacts of sub-aperture manufacturing techniques on the performance of freeform optics",

Proceedings ASPE/ASPEN Spring Topical Meeting: Manufacture and Metrology of Structured and Freeform Surfaces for Functional Applications, Paper 0061, p. 29 (2017).

12. E. L. Church and J. M. Zavada, "Residual surface roughness of diamond-turned optics," Appl. Opt. **14**, 1788-1795 (1975).

13. J. C. Stover, "Roughness characterization of smooth machined surfaces by light scattering," Appl. Opt. **14**, 1796-1802 (1975).

14. J. P. Marioge and S. Slansky, "Effect of figure and waviness on image quality," J. Opt. **14**, 189-198 (1983).

15. J. M. Tamkin, T. D. Milster, and William Dallas, "Theory of modulation transfer function artifacts due to mid-spatial-frequency errors and its application to optical tolerancing," Appl. Opt. **49**, 4825-4835 (2010).

16. J. M. Tamkin, "A Study of Image Artifacts Caused by Structured Mid-spatial Frequency Fabrication Errors on Optical Surfaces", Dissertation, The University of Arizona, (2010).

17. J. Filhaber, "Mid-spatial-frequency errors: the hidden culprit of poor optical performance", Laser Focus World **49(8)**, p. 32 (2013).

18. M. A. Alonso and G. W. Forbes, "Strehl ratio as the Fourier transform of a probability density of error differences," Opt. Lett. **41**, 3735-3738 (2016).

19. F. Tinker, K. Xin, "Correlation of mid-spatial features to image performance in aspheric mirrors," Proc. SPIE **8837**, 88370N (2013).

20. G. Boreman, *Modulation Transfer Function in Optical and Electro-Optical Systems*, (SPIE Press, 2001).

21. T. S. Ross, "Limitations and applicability of the Maréchal approximation," Appl. Opt. **48**, 1812-1818 (2009).

22. H. Aryan, C. J. Evans, and T. J. Suleski, "On the Use of ISO 10110-8 for Specification of Optical Surfaces with Mid-Spatial Frequency Errors," in Optical Design and Fabrication 2017 (Freeform, IODC, OFT), OSA Technical Digest (online) (Optical Society of America, 2017), paper OW4B.2.

23. W. J. Smith, *Modern Optical Engineering, 3rd ed.*, (McGraw-Hill, 2000), pp. 383–385.

24. B. Dube, R. Cicala, A. Closz, and J. P. Rolland, "How good is your lens? Assessing performance with MTF full-field displays," Appl. Opt. **56**, 5661-5667 (2017).

CHAPTER 4: SIMPLE METHODS FOR ESTIMATING THE PERFORMANCE AND
SPECIFICATION OF OPTICAL COMPONENTS WITH ANISOTROPIC MID-
SPATIAL FREQUENCY SURFACE ERRORS [42]

4.1 Abstract

Specification and tolerancing of surfaces with mid-spatial frequency (MSF) errors are

challenging and require new tools to augment simple surface statistics to better represent

the structured characteristics of these errors. A novel surface specification method is

developed by considering the structured and anisotropic nature of MSF errors and their

impact on the modulation transfer function (MTF). The result is an intuitive plot of

bandlimited RMS error values in polar coordinates which contains the surface error

anisotropy information and enables an easy to understand acceptance criterion. Methods,

application examples, and the connection of this surface specification approach to the MTF

are discussed.

4.2 Introduction

Mid-Spatial Frequency (MSF) surface errors are found between low-spatial frequency

'form' errors, and high-spatial frequency 'roughness' errors generally modeled with

scattering theory [1-3]. MSF errors are inherent to deterministic sub-aperture fabrication

techniques [4-11] and can appear on the surface with different structured signatures (e.g.

turned, milled, spiral) arising from the manufacturing method. Pseudo-random toolpaths

[7] can provide a means to reduce the impacts of MSF errors. While 'roughness' errors are

often random in distribution and scatter the light at large angles, MSF errors can be more

structured and diffract the light at angles small enough to directly illuminate the image plane [12].

From an optical characterization perspective, early statistical approaches and models for studying the impact of MSF errors required small perturbations, and errors were assumed to be random with no structured spatial frequencies in the Power Spectral Density (PSD) [13]. Marioge and Slansky [14], and more recently Tamkin [15,16] considered the impacts of structured MSF errors on optical performance. We recently published on characterization of the impacts of anisotropic MSF errors on the 2D modulation transfer function (2D MTF) [17,18]. The impacts of structured MSF errors, as discussed in the literature, can be complex and difficult to implement, so simple methods for estimating these impacts are desirable and of use from an engineering perspective. Youngworth and Stone [1] previously developed simple estimates for the effects of MSF errors on image quality under the assumption that the errors are isotropic. We build upon their work in this paper to provide similar tools for estimating the impacts of anisotropic MSF surface errors. We note that, for isotropic surfaces, our results converge to the estimates provided in [1].

There are multiple surface specification methods, with the root mean square (RMS) of surface height errors and Power Spectral Density (PSD) as the most common. Bandlimited RMS of surface height errors is widely used within the metrology, manufacturing, and optical design communities for specification of optical surfaces [1,2,19]. Since the RMS calculation is not sensitive to the shape or distribution of data and MSF signatures may have different anisotropic characteristics, MSF errors may not be sufficiently specified by a surface RMS value; *surfaces with the same RMS error but different manufacturing signatures can have different optical performance* [20]. Surfaces that pass a required RMS

specification may not yield the expected optical performance, which leads to confusion between designer and manufacturer. To overcome this issue, surfaces are often over-specified, which adds considerably to fabrication costs and cycle times. Hence, while RMS error is an effective specification for high-frequency errors [21], it is not a reliable method for MSF errors with anisotropic signatures.

Power spectral density (PSD) is another powerful method of surface specification. In optics, PSD has been used for specifying high-frequency surface errors to predict scattering properties of a surface [21-25] and has been applied to quantify the full spectrum of surface errors [26, 27]. The details of the PSD calculations are outside the scope of this paper but are well covered in the literature (e.g. [28,29]). The 2D PSD retains information on surface anisotropy, but these data are not easily connected to an optical performance criterion. The more commonly used 1D PSD representation is typically averaged over an orientation (e.g. horizontal, vertical, azimuthal), which loses information on anisotropy. Therefore, current methods of PSD specification are not conducive for use with anisotropic MSF errors [20]. We note that there are other ways that we benefit from the PSD in this work. In particular, PSD bandpass filters can be effectively utilized to separate MSF errors from form and roughness, and to calculate bandlimited RMS values from the volume underneath the 2D PSD of the surface within a given band [30].

In this paper, we propose a novel surface specification method for MSF errors to address the issues identified above. We quantify *directional* bandlimited RMS errors along different surface orientations in a polar representation and demonstrate connections to optical performance through the modulation transfer function (MTF) [31]. The proposed tool helps to facilitate a simple acceptance criterion to guarantee the performance of a

manufactured part, which is highly desirable but currently lacking for surfaces with anisotropic MSF errors.

In section 2, we describe the calculation methodology for the proposed surface specification. In section 3, we discuss the connection between the proposed surface specification to the MTF as an optical performance metric. Section 4 discusses methods for designers to define acceptance criteria after tolerancing. In this paper we focus on the MTF of optical components in a system and do not consider impacts of sensors or detectors.

4.3 Methodology of polar RMS specification

MTF is an effective optical performance metric for quantifying the impacts of MSF errors. In general, a surface RMS error leads to an optical phase difference from the perfect wavefront and reduces the average MTF of the system.

In order to establish a practical specification method for anisotropic surfaces with connections to optical performance, we seek to capture the directional RMS values that cause the largest reduction in MTF. To this end, we first calculate the individual RMS errors over multiple linear cross-sections on the surface error map at a specific orientation θ, as shown in Fig. 4-1. Note that this approach differs from taking the RMS over the entire error map at once. The directional calculations are repeated at different angles on the error map to capture the anisotropy. We choose to do this from 0 to 2π (rather than 0 to π) to generate a symmetric and more intuitive final plot in polar coordinates. We note that the calculation procedures must accommodate experimental data, which will normally be captured as rectangular grids through, for example, interferometric surface measurements. Processing and analyzing these data in a polar format will unavoidably require masking

and interpolation, which could introduce numerical artifacts. In particular, the analysis may be sensitive to local artifacts near the edge of the aperture where the data record is shorter. This issue could be mitigated, for example, by apodization, but such an approach also removes data and could introduce other numerical errors.
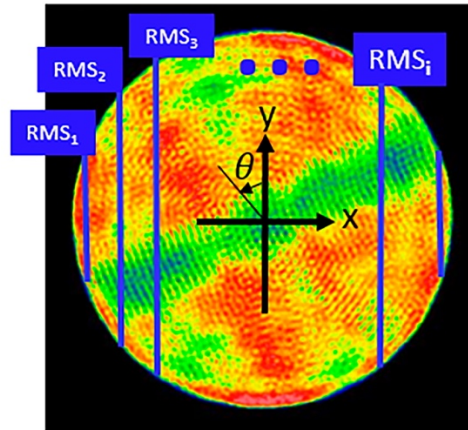
Figure 4-1: Calculating directional RMS values on a surface.

We then determine the *maximum* RMS value at a given orientation and plot this value as a function of θ in polar coordinates. The resulting *Polar RMS Plot (PRP)* captures both RMS error and anisotropy information. The word 'Polar' is chosen because results are plotted from 0 to 2π and should not be confused with an azimuthal analysis over an error map. Calculation procedures and assumptions for the PRP are discussed in more detail in Appendix I.

To demonstrate the PRP methodology, we consider two MSF errors with the same RMS error values (53 nm), but different signatures. Figure 4-2 shows two diamond-machined surfaces (turned and milled) synthesized in MATLAB using the same fabrication parameters: a tool-tip radius of 1 mm and Λ=5 μm, where Λ represents feed/rev for turning

and step-over for milling. A sinusoidal error with 150 nm peak to valley (PV) and 0.4 mm period was added to the resulting 'cusp-shaped' tool errors to approximate thermal drift effects from the tool chiller during manufacturing. A conventional RMS specification does not distinguish between the two surfaces, but their different anisotropy leads to different optical performance [18]. While the surface RMS values for both surfaces are equal, comparing the PRPs in Fig. 4-2(c) clearly shows differences between the two surfaces. We note that the directional periodic errors in Fig. 4-2(a) appear as distinctive peaks on the PRP in the same direction (in blue), while the PRP appears as a circle without any clear peaks (in solid red) for the rotationally symmetric errors in Fig. 4-2(b). We also note that for the turned texture (Fig. 4-2(b)) the incident light only sees a rotationally symmetric texture when on-axis; a directional texture is seen for off-axis field points or when the part is not positioned at the aperture stop.

Based on the PRP algorithm, it is expected to see peaks on the plots in the directions of the surface error periodicities. These peaks will appear wider for lower spatial frequency errors because longer spatial periods extend over several rotation angles, while higher frequency errors appear as sharper peaks. Thus, a quick look at the PRP can provide useful information about problematic surface errors.
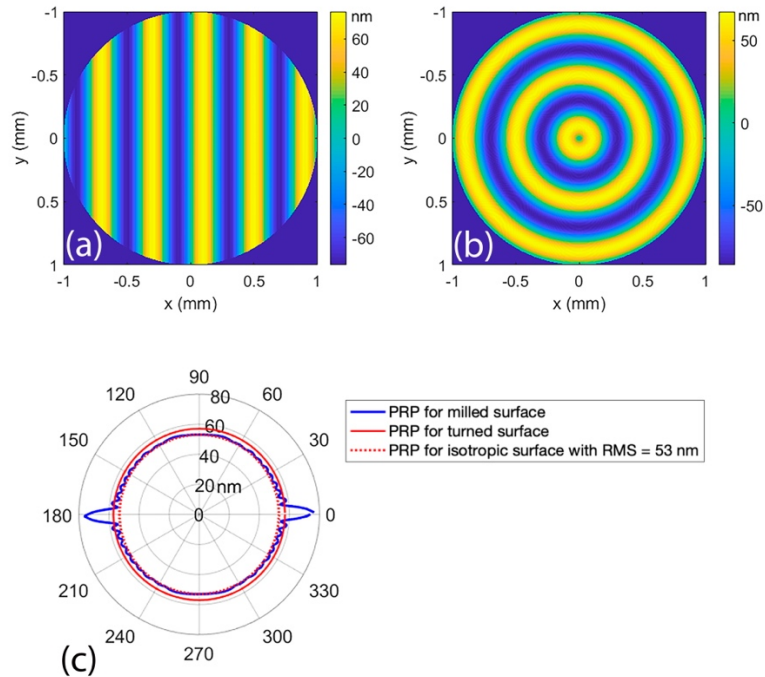
Fig. 4-2. (a) Raster-milled MSF error with RMS = 53 nm. (b) Turned MSF error with RMS = 53 nm. (c) Comparing PRPs for milled, turned, and isotropic surfaces with the same RMS.

In the next section, we discuss connections between the PRP and the MTF by making use of prior work by Youngworth and Stone in estimating the impacts of isotropic MSF errors on optical performance [1], and our recent introduction of the concept of a Minimum Modulation Curve (MMC) [17,18].

4.4 Connecting the PRP with the MTF

4.4.1 Estimates of the impact of isotropic MSF errors on optical performance

Historically, MSF errors have been primarily treated as random and isotropic. Youngworth and Stone [1] adopted a ray-based model to predict the effects of MSF errors on imaging systems at or near the diffraction limit. Despite its name, a ray-based model can include

diffraction effects by tracing the rays from an object point to specific points in the exit pupil where a phase map of the wave front is constructed. The wavefront can then be used to calculate the point spread function (PSF), optical transfer function (OTF), and other performance measures. Additionally, they employed perturbation methods to estimate the additional path lengths of rays due to the presence of MSF errors, introduced concepts from statistical optics, and made multiple assumptions about the nature of the MSF errors to enable simple estimates of the impacts of these MSF errors on image quality. The end result enables the wavefront variance to be approximated for a desired object field point as:

$$\sigma_\varphi^2 \cong -\left(\frac{2\pi}{\lambda}\right)^2 (\Delta n)^2 \sigma^2, \qquad (1.1)$$

where σ is the RMS surface error over the clear aperture, λ is the wavelength, and Δn is the difference between the refractive indices of the surface and the surrounding medium [1]. Therefore, the impacts of MSF errors on Strehl ratio (*SR*) and MTF can be estimated for isotropic surfaces as:

$$SR(\sigma) = Q(\sigma) SR_{diff} = Q(\sigma), \qquad (1.2)$$

$$MTF(\sigma) = Q(\sigma) MTF_{diff}. \qquad (1.3)$$

where

$$Q(\sigma) = \exp\left[-\left(\frac{2\pi}{\lambda}\right)^2 (\Delta n)^2 \sigma^2\right], \qquad (1.4)$$

and SR_{diff} (=1) and MTF_{diff} represent diffraction-limited performance for these two metrics.

We have introduced the idea of the PRP to better represent the impacts of anisotropic MSF errors on optical performance. In the following, we build on the work and assumptions of Youngworth and Stone [1] to demonstrate how substituting PRP_{max} (the amplitude of the largest PRP peak) instead of σ in Eqs. (4.1-4.4) connects the PRP to optical performance. Note that for an isotropic surface, $PRP_{max} = \sigma$ and therefore our estimates converge to those from Youngworth and Stone. However, we must first briefly review key concepts of the Minimum Modulation Curve (MMC).

4.4.2 The MMC and PRP for determining the impacts of anisotropic MSF errors

We recently introduced a new approach for 2D MTF analysis through the Minimum Modulation Curve (MMC) [17,18]. The MMC is a practical tool that summarizes key information from a 2D MTF in a more familiar 1D format. The MMC is defined as:

$$MMC(\rho) = \min_{\phi \in [0, 2\pi]} \left\{ MTF(\rho, \phi) \right\}, \tag{1.5}$$

where $MTF(\rho, \phi)$ is the MTF in polar coordinates, ρ is the radial spatial frequency, and ϕ is the azimuth angle measured from the horizontal. The minimum modulation values are chosen since MTF requirements are often given as the minimum acceptable modulation at specific spatial frequencies [16]. The MMC summarizes information from all orientations and is thus suitable for analyzing the impacts of anisotropic MSF structures. To illustrate the correlation between the MMC and the MTF estimated from the PRP, we substitute PRP_{max} in place of σ in Eqs. (4.3) and (4.4) to obtain:

$$MTF_{PRP} = Q\left(PRP_{\text{max}}\right)MTF_{\text{diff}}. \tag{1.6}$$

As an example, we consider a 2 mm diameter $f/5$ PMMA ($n = 1.4971$) lens at wavelength $\lambda = 486.1$ nm. We impose the MSF texture in Fig. 4-2(a) with $\sigma = 53$ nm on one side of this lens and simulate the PSF and MTF of the system via Fraunhofer diffraction theory [32]. Figure 4-3(a) compares the PRP of this surface (in solid blue) with the PRP of an isotropic surface (in dashed red) with the same RMS ($\sigma = 53$ nm). The blue PRP shows peaks up to $PRP_{max} = 76$ nm. As expected, the peaks are in the same direction as the periodicities of surface errors.

MTF simulation results in Fig. 4-3(a) confirm that the lens is not performing as predicted by Eq. (4.3) but does match the predictions from Eq. (4.6) based on the PRP. This simple example illustrates how overlooking the anisotropic nature of MSF errors could lead to an inaccurate specification. Note that both the MMC and the sagittal MTF drop below the red dashed acceptance line predicted for an isotropic MSF error. In Fig. 4-3(b), the PV of the sine error in Fig. 4-2(a) is reduced to 104 nm while keeping everything else the same. As a result, the PRP peak shrinks such that it just touches the dashed red circle representing an isotropic MSF surface error (so $PRP_{max} = \sigma$), and therefore the MMC and sagittal MTF of the lens are coincident with the MTF estimation lines. In Fig. 4-3(c), further reduction of the sine PV to 80 nm shrinks the PRP so that $PRP_{max} < \sigma$, which further improves the MTF. These results suggest that the PRP can serve as an intuitive, easy to understand tool for determining an acceptance criterion.
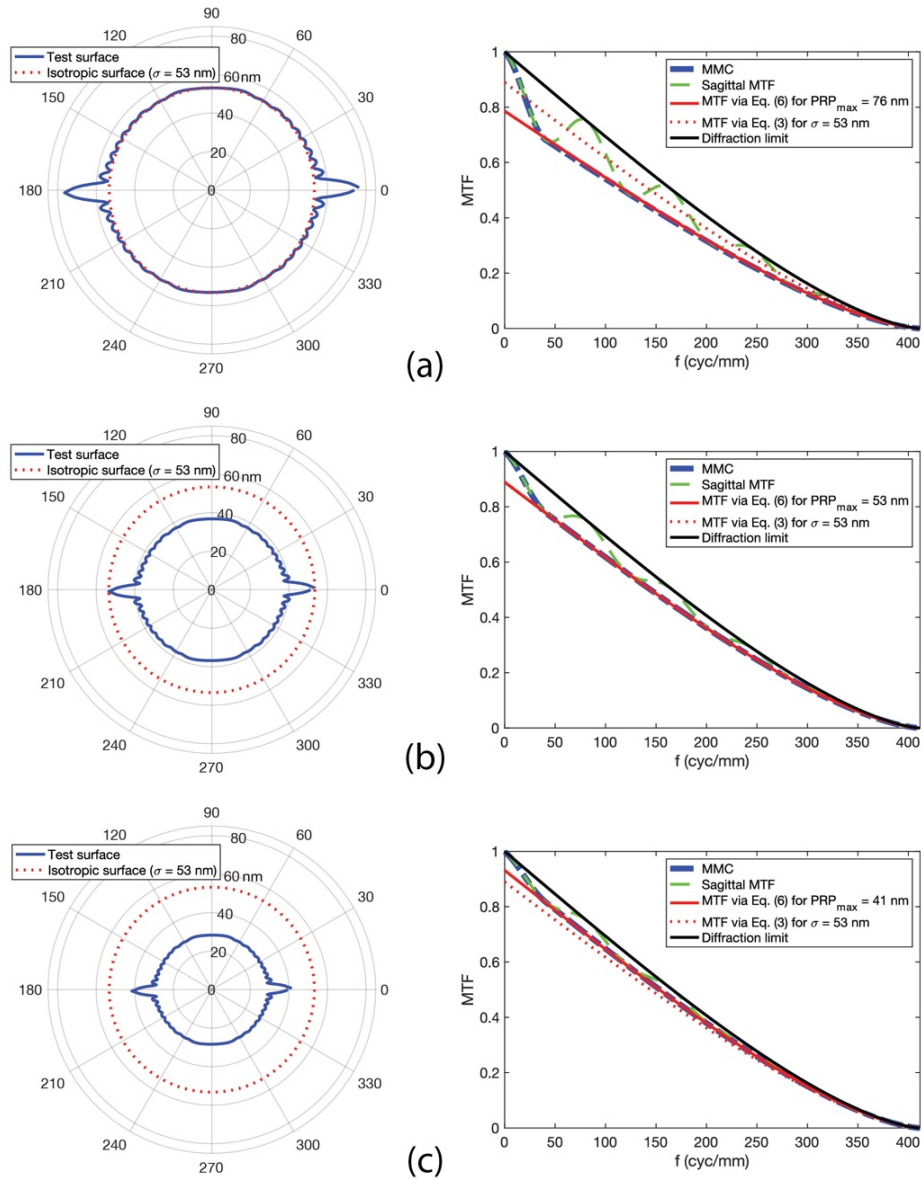
Figure 4-3: Comparison of PRP and MTF for simple lens with surface errors of the form in Fig. 4-1(a) with different amplitudes. (a) $\sigma = 53$ nm and $PRP_{max} = 76$ nm; (b) Effects of reducing the PV of the sinusoidal error to 104 nm ($\sigma = 37$ nm and $PRP_{max} = 53$ nm); and (c) Effects of reducing the PV of the sinusoidal error to 80 nm ($\sigma = 28$ nm and $PRP_{max} = 41$ nm).

The demonstrated relationship between PRP and MTF suggests that the PRP can provide

a practical means to assign effective specifications and acceptance criteria for optical

surfaces with MSF errors. The following section presents additional examples and proposes a simple method for estimating a required PRP_{max} for an optical specification.

4.5 PRP$_{max}$ as a surface specification

Optical designers are required to provide specifications on surface form, waviness (MSF errors), and roughness to manufacturers. In this section, we propose a method for calculating a PRP_{max} criterion for MSF errors after tolerancing a surface.

To this end, we again consider Eqs. (4.2) and (4.4) and note that the Strehl ratio in Eq. (4.2) equals the multiplicative factor $Q(\sigma)$ in Eq. (4.4) since $SR_{diff} = 1$. The SR is defined as the ratio of the central irradiance of an aberrated PSF to that of the unaberrated PSF. The SR can also be related to the Optical Transfer Function (OTF) [33]. For small aberrations (with negligible phase transfer functions), the OTF is equivalent to the MTF and we can write:

$$SR \equiv \frac{\iint MTF\left(f_x, f_y\right) df_x df_y}{\iint MTF_{diff}\left(f_x, f_y\right) df_x df_y}, \tag{1.7}$$

which is the ratio of the volume under the surface of the 2D MTF of an aberrated system to the volume under the 2D MTF of a diffraction-limited system. Eq. (4.7) can be represented in polar coordinates as:

$$SR \equiv \frac{\iint MTF(\rho,\phi) \; \rho \, d\rho \, d\phi}{\iint MTF_{diff}(\rho,\phi) \; \rho \, d\rho \, d\phi}; \tag{1.8}$$

We propose to use Eq. (4.8) with Eq. (4.5) to calculate a new value SR' that is analogous to SR but based on the MMC instead of MTF. We emphasize that SR' is <u>not</u> the traditional Strehl ratio:

$$SR' = \frac{\int MMC(\rho)\, d\rho}{\int MTF_{diff}(\rho)\, d\rho}. \tag{1.9}$$

The new performance parameter SR' is connected to the maximum wavefront variance and maximum RMS surface error (σ_{max}), since the MMC indicates the lowest modulation at each spatial frequency. Comparing Eqs. (4.2), (4.4), (4.8), and (4.9) suggests that we can set:

$$SR' = \exp\left[-\left(\frac{2\pi}{\lambda}\right)^2 (\Delta n)^2\, \sigma_{max}{}^2 \right] = Q', \tag{1.10}$$

and thus:

$$\sigma_{max} = \frac{\lambda}{2\pi\Delta n}\sqrt{-\log_e(Q')}, \tag{1.11}$$

where Q' is a new multiplicative factor analogous to Eq. (4.4) and which, considering Eq. (4.6), suggests that $\sigma_{max} \approx PRP_{max}$. Note that σ_{max} is calculated via the MMC where modulation equals one at zero spatial frequency, while PRP_{max} is connected to a linear estimate of the MTF through Eq. (4.6). As discussed below, this can cause differences between the values of σ_{max} and PRP_{max}, but the values are close empirically when the performance is close to diffraction-limited.

To better illustrate this point, we now consider several examples of MSF errors on the aforementioned lens used in Fig. 4-3 and compare the resulting MTF performances with predictions based on the methods discussed above. As shown in Fig. 4-4, Cases I and II correspond to simple sinusoidal signatures from raster milling and turning, respectively, while Cases III and IV contain multiple sinusoidal errors with different amplitudes and orientations. For each of these examples, we calculate the PRP from the MSF surface data and calculate the MMC following Eq. (4.5). We then calculate the acceptance line for MTF based on the isotropic assumptions of Youngworth and Stone [1] using Eq. (4.3), as well as MTF acceptance lines calculated based on PRP_{max} using Eq. (4.6), and based on σ_{max} from Eq. (4.11) in place of PRP_{max} in Eq. (4.6). The PV, period (Λ), and direction (θ) of the sinusoidal errors on each of surfaces are listed in Table 4-1. The calculated surface specifications for each example are listed in Table 4-2, and the corresponding MSF surfaces, PRPs, and MTF comparisons are shown in Fig. 4-5.
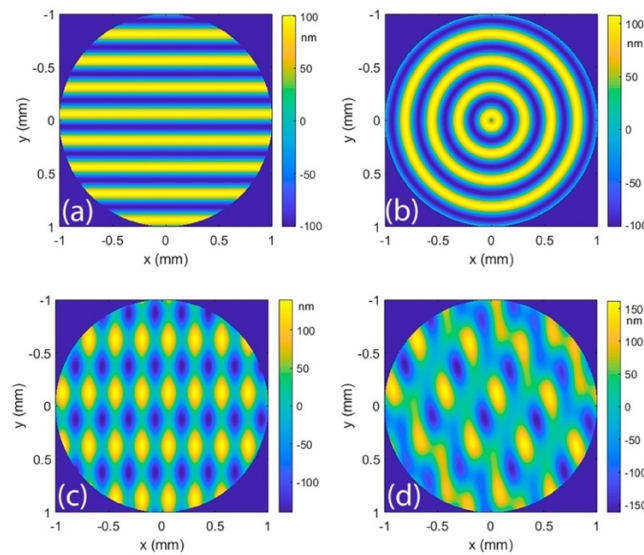

Fig. 4-4. Surface errors from Table (4-1): (a) Case I. (b) Case II. (c) Case III. (d) Case IV.

Table 4-1: List of sinusoidal errors for example surfaces in Fig. 4-4.

	PV_1 (nm)	Γ_1 (mm)	θ_1 (deg)	PV_2 (nm)	Γ_2 (mm)	θ_2 (deg)	PV_3 (nm)	Γ_3 (mm)	θ_3 (deg)
Case I	200	0.25	0	-	-	-	-	-	-
Case II	200	0.25	No	-	-	-	-	-	-
Case III	150	0.25	90	130	0.5	0	-	-	-
Case IV	100	0.25	90	75	0.5	0	150	0.4	60

Table 4-2: Calculated specification for example surfaces in Fig. 4-4.

	σ (nm)	σ_{max} (nm)	PRP_{max} (nm)	$Q = SR$	$Q' = SR'$
Case I	70	100	100	0.84	0.71
Case II	70	70	74	0.84	0.84
Case III	70	93	100	0.84	0.75
Case IV	70	93	101	0.84	0.75

We note that all four cases have the same σ, but do not have the same optical performance. For the rotationally symmetric example (Case II), the performance predicted by all methods is very close to that expected for an isotropic surface. However, the performance of surfaces with more anisotropy (Cases I, II, and IV) are consistently below the expectation for an isotropic surface. We also note that the MTF lines predicted via σ_{max} and PRP_{max} are very close and track well with the MMC.
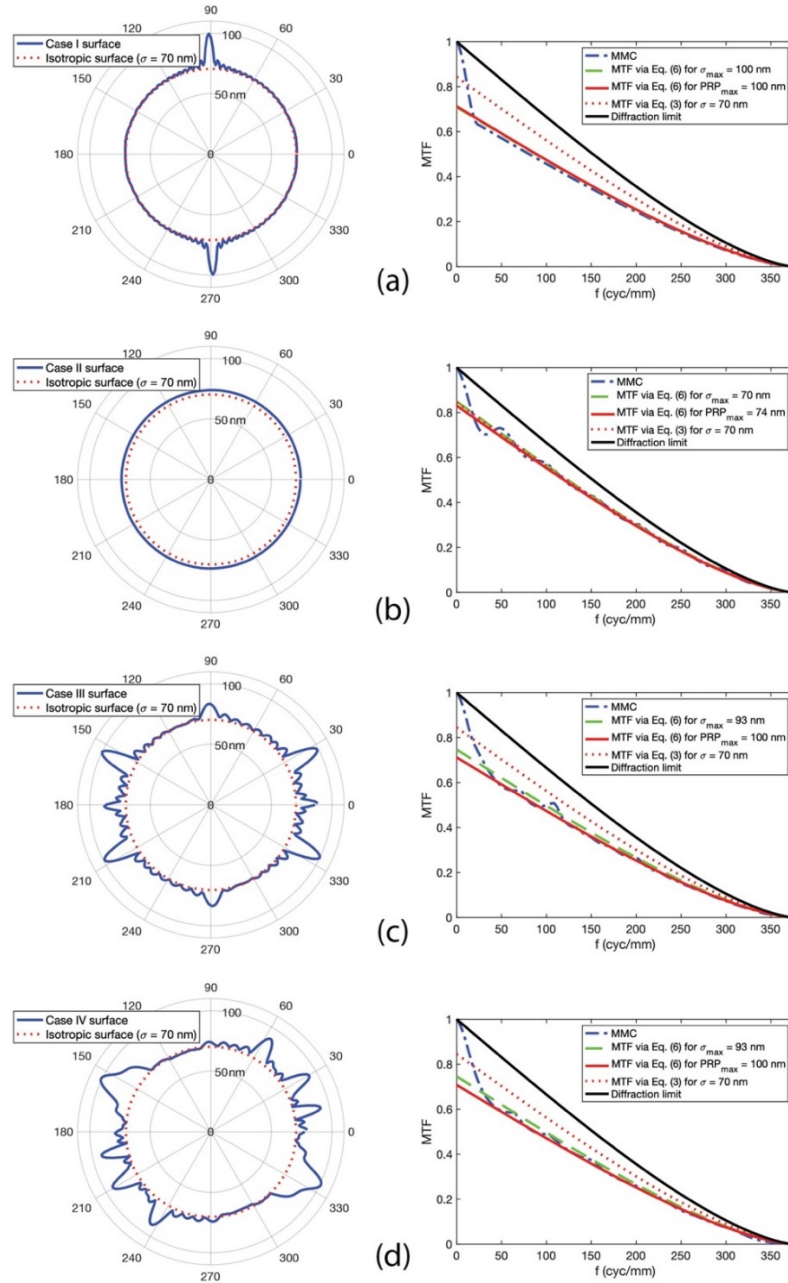
Figure 4-5: PRP and MTF simulations for (a) Case I, (b) Case II, (c) Case III, and (d) Case IV.

We now consider an additional example that demonstrates application to an experimental data set and also illustrates potential limitations of the proposed methodology. Figure 4-6(a) shows data from an experimental interferometric measurement of a surface created through a raster grinding process. It can be argued [2] that the low-

spatial frequency sinusoidal errors in the vertical direction should be considered to be form errors, rather than MSF errors; thus, the measurement result can be thought of as a 'non-ideal' surface with residual form errors after filtering the data. Figure 4-6(b) shows the PRP for this experimental surface, with large, wide peaks and large PV in the vertical direction corresponding to the low-spatial frequency errors. The measured RMS (σ) and PRP_{max} for this surface are 7 nm and 11 nm, respectively.

For optical simulations, we impose this surface error onto a f/10 mirror with 0.418 mm clear aperture at a wavelength of $\lambda = 157$ nm. We note that $\Delta n = 2n = 2$ in Eq. (4.2) for the reflective case in air since light reflects back into the same medium. Use of Eqs. (4.9) and (11) results in $\sigma_{max} = 8.7$ nm. The corresponding MTF simulations for this example are shown in Figure 4-6(c).
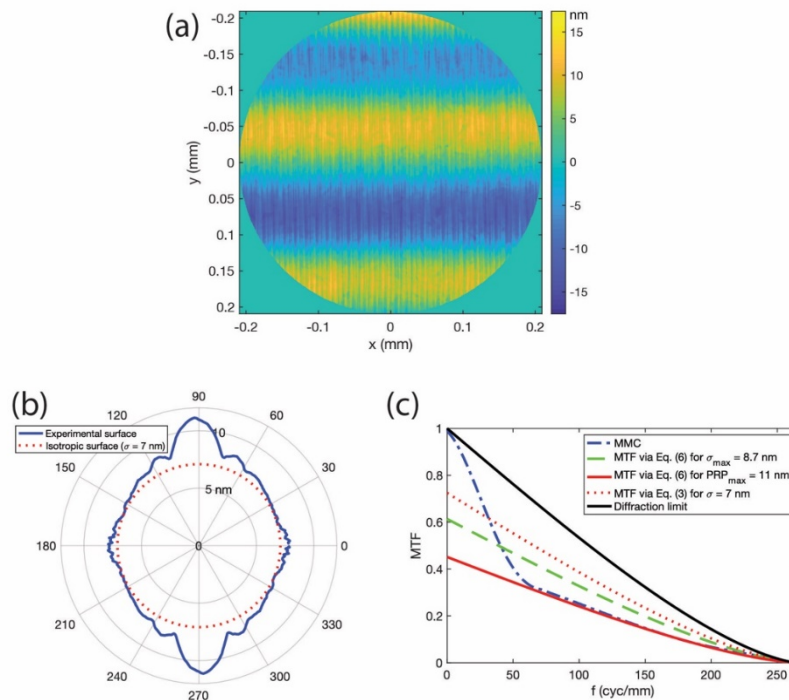

Fig. 4-6. (a) Example of experimental surface error from raster grinding on a mirror surface, and corresponding (b) PRP, and (c) MTF calculations for system operating at $\lambda = 157$ nm.

Multiple useful observations can be made from the simulations in Fig. 4-6(c). The MTF prediction from the experimentally determined PRP_{max} value from Fig. 4-6(b) tracks well with the MMC; the connection between the measured PRP and the MMC holds true even with the presence of the low-spatial frequency errors in the experimental surface data. However, the MTF line resulting from the calculated σ_{max} value shows a significant deviation from the MMC. This illustrates that the assumptions used in setting $PRP_{max} \approx \sigma_{max}$ are not valid in the presence of low-spatial frequency errors with PV values that are large in comparison to the MSF contributions. This makes sense, as such errors lead to drops in the MMC that introduce a bias in Eq. (4.9), resulting in $\sigma_{max} < PRP_{max}$. This bias is also observable at a lesser level in Figs. 4-5(c) and 4-5(d). However, we note that the predictions using σ_{max} still provides better estimates than values calculated via Eq. (4.3) for an isotropic surface.

To conclude this section, we note that Eq. (4.11) provides a simple method for designers to estimate PRP_{max} as an acceptance criterion after tolerancing optical system performance based on the MMC, subject to the assumptions and limitations discussed above. For example, if the aforementioned lens in Fig. 4-3 is required to have an MMC above 80% of the diffraction limit at all spatial frequencies, then $Q' = 0.8$ For this value of Q', Eq. (4.11) can be used to estimate $\sigma_{max} \approx PRP_{max} = 73$ nm. Even more simply, we assert that it would be reasonable for a designer who calculated a required value of σ (assuming an isotropic MSF error distribution) to provide that *same* numerical value as the PRP_{max} to the manufacturer as an acceptance criterion.

4.6 Discussion and Conclusion

We have proposed a novel method for specification of optical surfaces with anisotropic MSF surface errors based on the maximum RMS surface error in a given direction. Presenting the resulting data in polar coordinates results in a *Polar RMS Plot* (PRP) that enables a simple, intuitive acceptance criterion for anisotropic MSF surface errors. We have demonstrated connections between the maximum PRP value and the minimum optical modulation (MMC). The proposed methods provide a means to specify and set acceptance criteria for surfaces with anisotropic MSF errors. We note that, in the case of isotropic MSF surface errors, the proposed methods simplify to previously reported results [1]. In summary:

- The impacts of anisotropic distributions of MSF errors are captured by the MMC. The MMC can be estimated using Eq. (4.6) for a given PRP_{max}.
- Designers can estimate an acceptable PRP_{max} value for a surface via Eq. (4.11) and provide this value to manufacturers as a specification for MSF surface errors. This is in contrast to methods that provide a surface RMS value assuming isotropic error distributions and give unexpected performance results when anisotropic MSF errors are present.
- Manufacturers can use the PRP as a measurement tool and the PRP_{max} value as an acceptance criterion.

The intuitive PRP could also provide insights to manufacturers for process refinement and improvement. Since the PRP provides visual information on the orientation of surface errors and the widths of the peaks in the PRP are related to the spatial frequencies of those errors, the PRP and

PRP$_{max}$ may be useful in diagnosing processing issues that have the largest impacts on optical performance.

4.7 Appendix I: Procedure for calculating the Polar RMS Plot (PRP)

(1) Filter the desired mid-spatial frequency band using a PSD band-pass filter and save the new error map for processing.

(2) Apply an aperture to the error map to select the analysis area.

(3) Consider the surface height error map, *H(i, j)*, to be an N_x x N_y matrix. Calculate the RMS of real and non-zero values for each column of this matrix according to Fig. 4-1. Then pick the *maximum* RMS value between all columns.

(4) Rotate the surface error map by a small angle ($\Delta\theta$). In this paper, we chose one-degree angular increments and the nearest-neighbor interpolation method using the *imrotate.m* function in MATLAB.

(5) Repeat Steps 3 and 4 for each angle (θ) across the desired angular range. We chose to perform this calculation from 0 to 2π to enable an intuitive, symmetric final plot.

(6) Plot the maximum RMS value captured at each rotation angle of the surface error map with respect to each angle in polar coordinates.

Depending on the shape of incident beam footprint on the part, the user can apply a circular or rectangular aperture to the error map to select the analysis area. Although we have used a circular aperture in our calculations, the choice of aperture has not shown an impact on the overall PRP properties or its connection to optical performance. Choice of a

circular aperture is straightforward, but to apply a rectangular aperture, it is safer to crop down the surface area to $N/\sqrt{2}$ size, where $N = \min\{N_x, N_y\}$. This is suggested to avoid any noise leakage from the edges into the PRP data caused by the required matrix rotations in step (4).

The PRP resolution depends on the choice of angular increment ($\Delta\theta$) in rotating the surface error map. Surface resolution and the accuracy of the interpolation method used for rotating the surface matrix are other limiting factors. Similar to other surface specification methods, it is a good practice to mask large localized amplitude spikes within measured data to avoid unnecessary over-specification.

It is also important to remember that the position and diameter of the analysis on a measured part should be chosen based on the expected beam footprint within the design. It could be necessary to specify a part at different field angles. This helps to establish an effective specification connected to optical performance.

4.8 References

1. R. N. Youngworth and B. D. Stone, "Simple estimates for the effects of mid-spatial frequency surface errors on image quality", Appl. Opt. **39**(13), 2198-2209 (2000).

2. D. M. Aikens, J. E. DeGroote, and R. N. Youngworth, "Specification and Control of Mid-Spatial Frequency Wavefront Errors in Optical Systems," in *Frontiers in Optics 2008/Laser Science XXIV/Plasmonics and Metamaterials/Optical Fabrication and Testing, OSA Technical Digest (CD)* (Optical Society of America, 2008), paper OTuA1.

3. L. L. Deck and C. Evans, "High performance Fizeau and scanning white-light interferometers for mid-spatial frequency optical testing of free-form optics," Proc. SPIE **5921**, 59210A (2005).

4. H. Aryan, K. Liang, M. A. Alonso, T. J. Suleski, "Predictive models for the Strehl ratio of diamond-machined optics," Appl. Opt. **58**(12), 3272-3276 (2019).

5. R. Rhorer and C. Evans, "Fabrication of optics by diamond turning," in *Handbook of Optics, Third Edition Volume II: Design, Fabrication and Testing, Sources and Detectors, Radiometry and Photometry*, M. Bass, C. DeCusatis, J. Enoch, V. Lakshminarayanan, G. Li, C. Macdonald, V. Mahajan, and E. Van Stryland, eds. (McGraw-Hill, 2009), Chap. 10.

6. W. B. Lee, C. F. Cheung, and S. To, "Material-induced Vibration in Single Point Diamond Turning", in *Machining Dynamics*, K. Cheng, ed. (Springer, 2009), Chap. 9.

7. C. R. Dunn and D. D. Walker, "Pseudo-random tool paths for CNC sub-aperture polishing and other applications," Opt. Express **16**(23), 18942-18949 (2008).

8. A. Sohn, L. Lamonds, K. Garrard, "Modeling of Vibration in Single-Point Diamond Turning," in *Proceedings of the American Society of Precision Engineering* (ASPE, 2006), pp. 15-20.

9. G. W. Forbes, "Never-ending struggles with mid-spatial frequencies", Proc. SPIE **9525**, 95251B (2015).

10. Z. Hosseinimakarem, H. Aryan, A. Davies, and C. Evans, "Considering a Zernike polynomial representation for spatial frequency content of optical surfaces," in *Imaging and Applied Optics 2015, OSA Technical Digest (online)* (Optical Society of America, 2015), paper FT2B.2.

11. J. A. Shultz, H. Aryan, J. D. Owen, M. A. Davies, and T. J. Suleski, "Impacts of sub-aperture manufacturing techniques on the performance of freeform optics", in *Proceedings ASPE/ASPEN Spring Topical Meeting: Manufacture and Metrology of Structured and Freeform Surfaces for Functional Applications* (2017), paper 0061.

12. J. Filhaber, "Mid-spatial-frequency errors: the hidden culprit of poor optical performance", Laser Focus World **49**(8), 32 (2013).

13. E. L. Church and J. M. Zavada, "Residual surface roughness of diamond-turned optics," Appl. Opt. **14**(8), 1788-1795 (1975).

14. J. P. Marioge and S. Slansky, "Effect of figure and waviness on image quality," J. Opt. **14**(4), 189-198 (1983).

15. J. M. Tamkin, T. D. Milster, and William Dallas, "Theory of modulation transfer function artifacts due to mid-spatial-frequency errors and its application to optical tolerancing," Appl. Opt. **49**(25), 4825-4835 (2010).

16. J. M. Tamkin, "A Study of Image Artifacts Caused by Structured Mid-spatial Frequency Fabrication Errors on Optical Surfaces", Dissertation, The University of Arizona, (2010).

17. H. Aryan, T. J. Suleski, "Non-directional modulation transfer function for optical surfaces with asymmetric mid-spatial frequency errors", in *Optical Design and Fabrication 2019 (Freeform, OFT), OSA Technical Digest (online)* (Optical Society of America, 2019), paper OT1A.2.

18. H. Aryan, G. D. Boreman, and T. J. Suleski, "The Minimum Modulation Curve as a tool for specifying optical performance: application to surfaces with mid-spatial frequency errors," Opt. Express **27**(18), 25551-25559 (2019).

19. ISO 10110 Optics and photonics – Preparation of drawings for optical elements and systems. Part 8: Surface texture; roughness and waviness (2010).

20. H. Aryan, C. J. Evans, and T. J. Suleski, "On the Use of ISO 10110-8 for Specification of Optical Surfaces with Mid-Spatial Frequency Errors," in *Optical Design and Fabrication 2017 (Freeform, IODC, OFT), OSA Technical Digest (online)* (Optical Society of America, 2017), paper OW4B.2.

21. J. C. Stover, *Optical Scattering: Measurement and Analysis, 2ⁿᵈ Edition* (SPIE, 1995), Chap. 2.

22. J. E. Harvey, "X-ray optics," in *Handbook of Optics, 2nd Edition Volume II: Devices, Measurements, and Properties*, M. Bass, E. Van Stryland, D. R. Williams, and W. L. Wolfe, eds. (McGraw-Hill, 1995), Chap. 11.

23. J. M. Bennett and L. Mattsson, *Introduction to Surface Roughness and Scattering, 2ⁿᵈ Edition* (Optical Society of America, 1999).

24. J. M. Elson and J. M. Bennett, "Calculation of the power spectral density from surface profile data," Appl. Opt. **34**(1), 201-208 (1995).

25. A. Duparré, J. Ferre-Borrull, S. Gliech, G. Notni, J. Steinert, and J. Bennett, "Surface characterization techniques for determining the root-mean-square roughness and power spectral densities of optical components," Appl. Opt. **41**(1), 154-171 (2002).

26. D. M. Aikens, C. R. Wolfe, and J. K. Lawson, "The use of Power Spectral Density (PSD) functions in specifying optics for the National Ignition Facility," Proc. SPIE **2576**, 281-292 (1995).

27. J. K. Lawson, C. R. Wolfe, K. R. Manes, J. B. Trenholme, D. M. Aikens, and R. E. English, Jr., "Specification of optical components using the power spectral density function," Proc. SPIE **2536**, 38-50 (1995).

28. R. N. Youngworth, B. B. Gallagher, and B. L. Stamper, "An overview of power spectral density (PSD) calculations," Proc. SPIE **5869**, 58690U (2005).

29. E. Sidick, "Power spectral density specification and analysis of large optical surfaces," Proc. SPIE **7390**, 73900L (2009).

30. Zygo Corp., "Data processing: Using the filter PSD plot", in *Mx Help* (Zygo, 2015).

31. G. Boreman, *Modulation Transfer Function in Optical and Electro-Optical Systems* (SPIE, 2001), Chap. 1.

32. J.W. Goodman, *Introduction to Fourier Optics* (Roberts and Company, 2005), Chap. 5.

33. J.W. Goodman, *Introduction to Fourier Optics* (Roberts and Company, 2005), Chap. 6.

34. H. Aryan, T. J. Suleski, "Specification of Optical Surfaces with Anisotropic Mid-Spatial Frequency Errors", in *Optical Design and Fabrication 2019 (Freeform, IODC, OFT), OSA Technical Digest (online)* (Optical Society of America, 2019), paper OM4A.5.

CHAPTER 5: CONCLUSION

5.1 Summary of Work

Specification of optical surfaces with mid-spatial frequency (MSF) errors is a challenging task because of the demand for a simple solution to a complex problem. Commonly used surface specification methods are not able to capture many important characteristics of MSF errors.

Diamond-machined MSF errors were investigated more specifically in article one [40]. Predictive models were developed for the Strehl ratio of these surfaces based on a targeted optical performance. These models could help determine manufacturing parameters for balancing the impact of diamond cusp errors with manufacturing costs. However, this works also illustrated that conventional performance metrics like the Strehl ratio and conventional surface specification metrics such as surface RMS are not adequate for surfaces with anisotropic MSF errors.

An important step toward developing tolerancing strategies within a design is to first develop tools that are able to effectively characterize the impact of MSF errors on the optical performance. Multiple optical performance metrics were analyzed for various optical systems. In our study, 2D MTF was shown to be the most promising metric for observing the impact of MSF errors. Therefore, in article two [41], a non-directional analysis approach for 2D-MTF was proposed which is also useful for systems with rotationally asymmetric performance. This approach summarizes key information within a complex 2D-MTF and presents it in 1D familiar formats through the minimum modulation curve (MMC) and the standard deviation of the modulation σ_{MTF}.

In article three [42], we developed a novel surface specification method in which quantifies the surface RMS and anisotropy distribution of errors at the same time. This method provides an intuitive specification plot which illustrates a strong connection to the optical performance of a part through the modulation transfer function (MTF).

Thus, tools developed in article two [41] and three [42] provide a closed loop for true MSF specification and characterization of the impact which facilitates the long-term problem of MSF testing and tolerancing.

5.2 Future work

1. Experimental implementation of the predictive models in article one [40] for optimizing the diamond machining fabrication process. The performance of a fabricated part could be validated using an MTF/PSF bench.

2. To date, the Polar RMS Plot method in article three [42] has been applied to several experimentally measured surface data sets. Also, the minimum modulation curve (MMC) has been applied to simulated optical performance models from these measured surface data. It is desirable that both tools be utilized experimentally and the connection between the two be illustrated and validated experimentally.

3. The polar RMS plot, in article three [42], could be investigated further to extract more surface characteristics from the plots such as the spatial frequency and peak to valley (PV) of surface errors.

4. The methodology of the MMC calculation [41] could be adapted to drive a new method for analyzing 2D PSD data. One possibility is to pick the maximum power for each spatial frequency in an azimuthal analysis approach.

5. Tolerancing surface errors with respect to the MMC [41], by using optical design codes such as Zemax or CODE V, to define surface acceptance criteria, could be another practical and useful research area.

REFERENCES:

1. R. J. Noll, "Effect of Mid- and High-Spatial Frequencies on Optical Performance," Opt. Eng. 18(2) 182137 (1 April 1979).

2. G. W. Forbes, "Never-ending struggles with mid-spatial frequencies", Proc. of SPIE Vol. 9525, 95251B (2015).

3. M. Bass, C. DeCusatis, J. Enoch, V. Lakshminarayanan, G. Li, C. Macdonald, V. Mahajan, and E. V. Stryland. *Handbook of Optics, Third Edition Volume II: Design, Fabrication and Testing, Sources and Detectors, Radiometry and Photometry*. (McGraw-Hill, 2009), Chap. 10.

4. T. T. Saito, "Machining of optics: an introduction," Appl. Opt. **14**, 1773-1776 (1975).

5. K. Smith, R. Winger, A. H. Lettington, and P. F. T. C. Stillwell, "Diamond turning of mirrors and infrared optical components", Journal of Physics D: Applied Physics **21** (10S): S67 (2000).

6. M. N. Cheng, C. F. Cheung, W. B. Lee, S. To, "A study of factors affecting surface quality in ultra-precision raster milling", Key Engineering Materials 339:400-406 (2007).

7. S. Rakuff and P. Beaudet, "Thermal and structural deformations during diamond turning of rotationally symmetric structured surfaces", Journal of Manufacturing Science and Engineering **130**(4) (2008).

8. James E. Harvey, "Integrating optical fabrication and metrology into the optical design process," Appl. Opt. **54**, 2224-2233 (2015).

9. D. M. Aikens, J. E. DeGroote, and R. N. Youngworth, "Specification and Control of Mid-Spatial Frequency Wavefront Errors in Optical Systems", in Frontiers in Optics 2008/Laser Science XXIV/Plasmonics and Metamaterials/Optical Fabrication and Testing, OSA Technical Digest (CD) (Optical Society of America, 2008), paper OTuA1.

10. J. Filhaber, "Mid-spatial-frequency errors: the hidden culprit of poor optical performance", Laser Focus World **49**(8), p. 32 (2013).

11. J. M. Tamkin, W. J. Dallas, and T. D. Milster, "Theory of point-spread function artifacts due to structured mid-spatial frequency surface errors", App. Opt. **49**, 4814-4824 (2010).

12. J. M. Tamkin, T. D. Milster, and W. J. Dallas, "Theory of modulation transfer function artifacts due to mid-spatial-frequency errors and its application to optical tolerancing", Appl. Opt. **49**, 4825-4835 (2010).

13. J. M. Tamkin, "A Study of Image Artifacts Caused by Structured Mid-spatial Frequency Fabrication Errors on Optical Surfaces", Dissertation, The University of Arizona (2010).

14. R. N. Youngworth and B. D. Stone, "Simple estimates for the effects of mid-spatial frequency surface errors on image quality", Applied Optics **39** (13), 2198-2209 (2000).

15. D. Martínez-Galarce, J. Harvey, M. Bruner, J. Lemen, E. Gullikson, R. Soufli, E. Prast, S. Khatri, "A novel forward-model technique for estimating EUV imaging performance: design and analysis of the SUVI telescope", Proc. SPIE 7732, Space

Telescopes and Instrumentation 2010: Ultraviolet to Gamma Ray, 773237 (29 July 2010).

16. J. E. Harvey, N. Choi, A. Krywonos, J. G. Marcen, "Calculating BRDFs from surface PSDs for moderately rough optical surfaces", Proc. SPIE 7426, Optical Manufacturing and Testing VIII, 74260I (9 September 2009).

17. J. E. Harvey, N. Choi, S. Schroeder, A. Duparré, "Total integrated scatter from surfaces with arbitrary roughness, correlation widths, and incident angles", Opt. Eng. **51**(1) 013402 (2012).

18. J. E. Harvey, N. Choi, A. Krywonos, and G. Peterson, "Predicting Image Degradation from Optical Surface Metrology Data", in International Optical Design Conference and Optical Fabrication and Testing, OSA Technical Digest (CD) (Optical Society of America, 2010), paper OMB2.

19. James E. Harvey, "Integrating optical fabrication and metrology into the optical design process", Appl. Opt. **54**, 2224-2233 (2015).

20. James E Harvey, "Parametric analysis of the effect of scattered light upon the modulation transfer function", Proc. SPIE 8841, Current Developments in Lens Design and Optical Engineering XIV, 88410W (25 September 2013).

21. H. E. Bennett and J. O. Porteus, "Relation Between Surface Roughness and Specular Reflectance at Normal Incidence", J. Opt. Soc. Am. **51**, 123-129 (1961).

22. E. L. Church and J. M. Zavada, "Residual surface roughness of diamond-turned optics", Appl. Opt. **14**, 1788-1795 (1975).

23. J. C. Stover, "Roughness characterization of smooth machined surfaces by light scattering", Appl. Opt. **14**, 1796-1802 (1975).

24. J. P. Marioge and S. Slansky, "Effect of figure and waviness on image quality", Journal of Optics **14**, 189-198 (1983).

25. M. A. Alonso and G. W. Forbes, "Strehl ratio as the Fourier transform of a probability density of error differences," Opt. Lett. **41**, 3735-3738 (2016).

26. K. Liang and M. A. Alonso, "Understanding the effects of groove structures on the MTF", Opt. Exp. **25**, 18827-18841 (2017)

27. A. M. Hvisc, J. H. Burge, "Structure function analysis of mirror fabrication and support errors", Proc. SPIE 6671, Optical Manufacturing and Testing VII, 66710A (14 September 2007).

28. R. E. Parks, "Specifications: Figure and Finish are not enough", Proc. of SPIE Vol. 7071, 70710B, (2008).

29. D. J. Markason, "Controlling surface figure errors of optical components," Proc. SPIE 7652, International Optical Design Conference 2010, 76521A (9 September 2010).

30. L. He, C. J Evans, and A. Davies, "Spatial content analysis for precision surfaces with the area structure function", IOP Publishing, Surface Topography: Metrology and Properties, Vol. **2**, Nu. 1 (2013).

31. L. He, C. J. Evans, and A. Davies, "Two-quadrant area structure function analysis for optical surface characterization," Opt. Exp. **20**, 23275-23280 (2012).

32. L. He, A. Davies, C. J. Evans, "Comparison of the area structure function to alternate approaches for optical surface characterization", Proc. SPIE 8493, Interferometry XVI: Techniques and Analysis, 84930C (13 September 2012).

33. Z. Hosseinimakarem, H. Aryan, A. Davies, and C. Evans, "Considering a Zernike polynomial representation for spatial frequency content of optical surfaces," in Imaging and Applied Optics 2015, OSA Technical Digest (online) (Optical Society of America, 2015), paper FT2B.2.

34. Z. Hosseinimakarem, A. D. Davies, C. J. Evans, "Zernike polynomials for mid-spatial frequency representation on optical surfaces," Proc. SPIE 9961, Reflection, Scattering, and Diffraction from Surfaces V, 99610P (26 September 2016).

35. Z. Hosseinimakarem, A. D. Davies, C. J. Evans, "Usefulness of orthogonal basis sets for predicting optical performance of wavefronts with mid-spatial frequency error," Proc. SPIE 10373, Applied Optical Metrology II, 1037302 (23 August 2017).

36. G. Forbes, "Detrending on Steroids… MSF Characterization via Freeform Polynomials," in Renewable Energy and the Environment, OSA Technical Digest (online) (Optical Society of America, 2013), paper FM2B.1.

37. C. R. Dunn and D. D. Walker, "Pseudo-random tool paths for CNC sub-aperture polishing and other applications," Opt. Exp. **16**, 18942-18949 (2008).

38. J. DeGroote Nelson, A. Gould, C. Klinger, and M. Mandina "Incorporating VIBE into the precision optics manufacturing process", Proc. SPIE 8126, Optical Manufacturing and Testing IX, 812613 (27 September 2011).

39. X. Guo, Y. Shu, G. Kim, M. Palmer, H. Choi, D. Wook Kim, "Pseudorandom orbiting stroke for freeform optics postprocessing," Opt. Eng. 58(9) 092608 (17 April 2019).

40. H. Aryan, K. Liang, M. A. Alonso, and T. J. Suleski, "Predictive models for the Strehl ratio of diamond-machined optics," Appl. Opt. **58**, 3272-3276 (2019).

41. H. Aryan, G. D. Boreman, and T. J. Suleski, "The Minimum Modulation Curve as a tool for specifying optical performance: application to surfaces with mid-spatial frequency errors," Opt. Express **27**, 25551-25559 (2019).

42. H. Aryan, G. D. Boreman, and T. J. Suleski, "Simple methods for estimating the performance and specification of optical components with anisotropic mid-spatial frequency surface errors," Opt. Exp. **27**, 32709-32721 (2019).

43. J. W. Goodman, *Introduction to Fourier Optics* (Roberts and Company, 2005).

44. D. G. Smith, *Field Guide to Physical Optics* (SPIE, 2013).

45. G. Boreman, *Modulation Transfer Function in Optical and Electro-Optical Systems* (SPIE Press, 2001).

46. M. Born and E. Wolf, *Principles of Optics, 5th ed.* (Pergamon Press, Oxford 1975).

47. J. C. Juarez, D. M. Brown, D. W. Young, "Strehl ratio simulation results under strong turbulence conditions for actively compensated free-space optical communication systems," Proc. SPIE 8732, Atmospheric Propagation X, 873207 (17 May 2013).

48. H. Aryan, C. J. Evans, and T. J. Suleski, "On the Use of ISO 10110-8 for Specification of Optical Surfaces with Mid-Spatial Frequency Errors", in Optical Design and Fabrication 2017 (Freeform, IODC, OFT), OSA Technical Digest (online) (Optical Society of America, 2017), paper OW4B.2.

49. J. V. Baliga, B. D. Cohn, "Simplified Method For Calculating Encircled Energy", Proc. SPIE 0892, Simulation and Modeling of Optical Systems, (9 June 1988).

50. H. Aryan, T. J. Suleski, "Non-directional modulation transfer function for optical surfaces with asymmetric mid-spatial frequency errors", in Optical Design and Fabrication 2019 (Freeform, OFT), OSA Technical Digest (online) (Optical Society of America, 2019), paper OT1A.2.

51. J. C. Stover, *Optical Scattering* (McGraw-Hill, 1990).

52. J. E. Harvey, "X-ray optics", *in Handbook of Optics, 2nd Ed.* (Optical Society of America, 1995), Vol. 2, Chap. 11.

53. J. M. Bennett and L. Mattsson, *Introduction to Surface Roughness and Scattering 2nd Ed.* (Optical Society of America, 1999).

54. J. M. Elson and J. M. Bennett, "Calculation of the power spectral density from surface profile data," Appl. Optics **34**, 201-208 (1995).

55. Duparré, J. Ferre-Borrull, S. Gliech, G. Notni, J. Steinert, J. Bennett, "Surface characterization techniques for determining the root-mean-square roughness and power spectral densities of optical components", Applied Optics **41**, pp. 154-171, 2002.

56. D. M. Aikens, C. R. Wolfe, J. K. Lawson, "Use of power spectral density (PSD) functions in specifying optics for the National Ignition Facility", Proc. SPIE 2576, International Conference on Optical Fabrication and Testing, (2 August 1995).

57. J. K. Lawson, C. R. Wolfe, K. R. Manes, J. B. Trenholme, D. M. Aikens, R. E. English Jr., "Specification of optical components using the power spectral density function", Proc. SPIE 2536, Optical Manufacturing and Testing, (8 September 1995).

58. Data processing: Using the filter PSD plot, Mx Help (Zygo Corporation).

59. R. N. Youngworth, B. B. Gallagher, B. L. Stamper, "An overview of power spectral density (PSD) calculations," Proc. SPIE 5869, Optical Manufacturing and Testing VI, 58690U (18 August 2005).

60. E. Sidick, "Power spectral density specification and analysis of large optical surfaces", Proc. SPIE 7390, Modeling Aspects in Optical Metrology II, 73900L (17 June 2009).

61. ISO 10110 Optics and photonics – Preparation of drawings for optical elements and systems. Part 8: Surface texture; roughness and waviness (2010).

62. J. J. Kumler, J. B. Caldwell, "Measuring surface slope error on precision aspheres", Proc. SPIE 6671, Optical Manufacturing and Testing VII, 66710U (14 September 2007).